NASA TECHNICAL NOTE




NASA TN D-6605

# EFFECTS OF SPECIFIC SPEED ON EXPERIMENTAL PERFORMANCE OF A RADIAL-INFLOW TURBINE

*by Milton G. Kofskey and William J. Nusbaum*

*Lewis Research Center*
*Cleveland, Ohio 44135*

NATIONAL AERONAUTICS AND SPACE ADMINISTRATION • WASHINGTON, D. C. • FEBRUARY 1972

| 1. Report No. | 2. Government Accession No. | 3. Recipient's Catalog No. |
|---|---|---|
| NASA TN D-6605 | | |

| 4. Title and Subtitle | 5. Report Date |
|---|---|
| EFFECTS OF SPECIFIC SPEED ON EXPERIMENTAL PERFORMANCE OF A RADIAL-INFLOW TURBINE | February 1972 |
| | 6. Performing Organization Code |
| 7. Author(s) | 8. Performing Organization Report No. |
| Milton G. Kofskey and William J. Nusbaum | E-6349 |
| | 10. Work Unit No. |
| 9. Performing Organization Name and Address | 112-27 |
| Lewis Research Center<br>National Aeronautics and Space Administration<br>Cleveland, Ohio 44135 | 11. Contract or Grant No. |
| | 13. Type of Report and Period Covered |
| 12. Sponsoring Agency Name and Address | Technical Note |
| National Aeronautics and Space Administration<br>Washington, D.C. 20546 | 14. Sponsoring Agency Code |

15. Supplementary Notes

This report supersedes NASA TN D-6182

16. Abstract

The performance of a 12.62-cm (4.97-in.) tip diameter radial-inflow turbine was investigated over a range of specific speeds from 0.28 to 0.73 (39 to 94) at equivalent design speed and pressure ratio. The specific speed range was obtained by using stators with different throat areas. The stators were used with the design rotor, with a rotor exducer extension that reduced the rotor throat area, and with the rotor exducer cut back to increase the rotor throat area. The efficiencies obtained with the three rotor configurations are presented and compared.

| 17. Key Words (Suggested by Author(s)) | 18. Distribution Statement |
|---|---|
| Radial flow turbines; Performance tests; Specific speed; Efficiency; Comparison; Investigation | Unclassified - unlimited |

| 19. Security Classif. (of this report) | 20. Security Classif. (of this page) | 21. No. of Pages | 22. Price* |
|---|---|---|---|
| Unclassified | Unclassified | 43 | $3.00 |

* For sale by the National Technical Information Service, Springfield, Virginia 22151

# EFFECTS OF SPECIFIC SPEED ON EXPERIMENTAL PERFORMANCE OF A RADIAL-INFLOW TURBINE

by Milton G. Kofskey and William J. Nusbaum

Lewis Research Center

## SUMMARY

An experimental cold-air investigation was made to determine the effect of specific speed on the performance of a 12.62-cm (4.97-in.) tip diameter radial-inflow turbine. The range of specific speeds investigated, 0.28 to 0.73 (36 to 94 $(rpm)(ft^{3/4})/(sec)^{1/2}$) at equivalent design speed and pressure ratio, was obtained by changing the volume flow using stators with different throat areas. The stators were used with the design rotor, with a rotor extension that reduced rotor throat area, and with a cutback of the rotor exit, which increased the rotor throat area.

Results showed that total efficiencies of 0.90 and greater can be obtained over a large specific speed range of 0.37 to 0.80 (48 to 104). Similarly, static efficiencies of 0.85 or greater can be obtained over the specific speed range of 0.34 to 0.72 (44 to 94). The results indicated that, if high efficiency is desired over a large range of specific speeds, optimum stator-rotor throat area ratio should be maintained when stator throat area is changed.

A maximum total efficiency of 0.925 was obtained over the specific speed range of 0.42 to 0.65 (55 to 85). The maximum static efficiency of 0.91 was obtained at a specific speed of about 0.43 (56).

Rotor exit flow angle surveys along with calculated blade surface velocities indicated possible flow separation in the rotor hub region with the 20-percent stator configuration.

## INTRODUCTION

The development of high-speed turbomachinery for long life and high reliability is a long and expensive process, especially in the case of gas bearing machines for space-power application. It is, therefore, desirable to use a given basic machine for a variety

of systems and system power levels. The desired flexibility of operation can be accomplished by varying system pressure level, by varying flow areas in the compressor and turbine, or by some combination of these. Variation of flow area has advantages in duct sizing, packaging, and system pressure drops because system pressure level can be maintained at a maximum value for a range of power levels.

The operation of a radial inflow turbine with various stator throat areas has been examined previously; the experimental results are published in reference 1. This investigation indicated that efficiency is highest over a narrow range of specific speeds, and it then decreases toward both ends of the range investigated. It was stated in the reference that use of the same rotor for all stator configurations investigated could have resulted in the efficiencies decreasing toward the extremes of the specific speed range.

The work described herein employed the 12.62-centimeter (4.97-in.) tip diameter turbine of reference 2. The specific speed range investigated covered values well above and below the design value. Stators with throat areas from 20 to 144 percent of design were used with the rotor as designed. In addition, an extension of the rotor exducer, which reduced the rotor throat area to 53 percent of design, and a cut-back rotor to provide a rotor throat area of 137 percent of design were employed in order to better match the stator and rotor throat areas at the extremes of the specific speed range. Performance was measured at design speed and over a range of pressure ratio. Inlet pressure for each configuration was selected to provide design Reynolds number at design speed and pressure ratio. Rotor channel velocities were calculated for each configuration to provide an indication of changes in blade loading with changes in geometry at design speed and pressure ratio. Also, a loss breakdown was determined for several configurations.

## TURBINE DESCRIPTION

The 12.62-centimeter (4.97-in.) tip diameter radial inflow turbine used in this investigation is described in reference 2. Equivalent design requirements are as follows (the symbols are defined in appendix A):

| | |
|---|---|
| Mass flow, $\epsilon w\sqrt{\theta_{cr}}/\delta$, kg/sec; lb/sec | 0.2204, 0.4860 |
| Specific work, $\Delta h/\theta_{cr}$, J/g; Btu/lb | 34.50; 14.82 |
| Rotative speed, $N\sqrt{\theta_{cr}}$, rpm | 29687 |
| Total- to static-pressure ratio, $p_1'/p_3$ | 1.695 |
| Blade-jet speed ratio, $\nu$ | 0.690 |
| Specific speed, $N_s = NQ^{1/2}/(H')^{3/4}$, dimensionless; $(rpm)(ft^{3/4})/sec^{1/2}$ | 0.59, 76 |

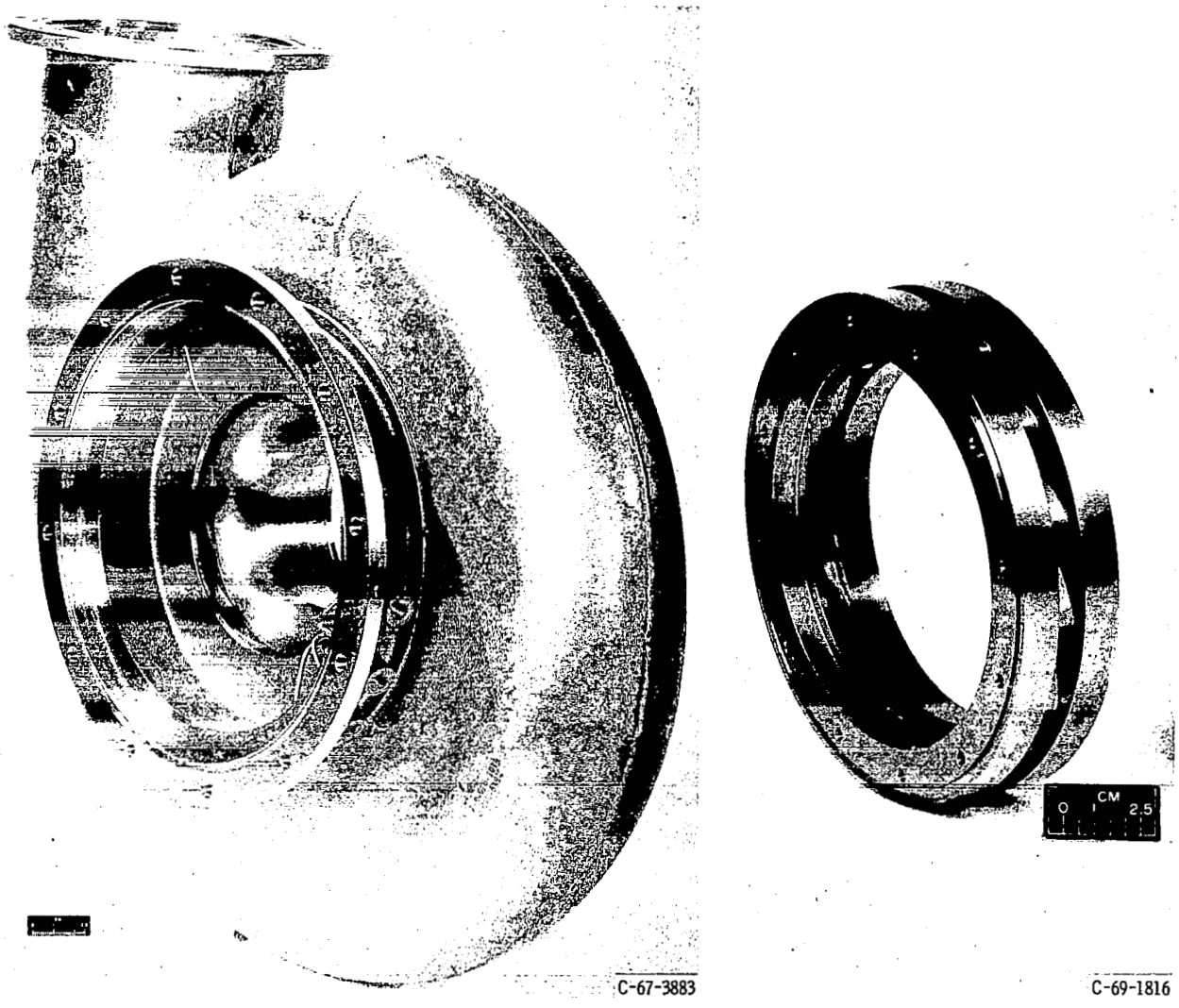


(a) Scroll-stator assembly.

(b) Stator configuration.

Figure 1. - Scroll-stator assembly and typical stator configuration.

The range of specific speeds at equivalent design speed and pressure ratio was obtained by changing volume flow, using stators of different throat areas. This was done by using the same blade profile and changing the blade setting angle and blade number. Five additional stators having throat areas of 20, 42, 66, 125, and 144 percent of design were used to cover a specific speed range of 0.28 to 0.73 (39 to 94). Along with these stator modifications, modifications of the rotor were also investigated. An extended rotor exducer was designed to provide 53 percent of the design rotor throat area. This extension would provide a better match of the stator and rotor throat areas for the 66-, 42-, and 20-percent stator configurations. When tests with these configurations

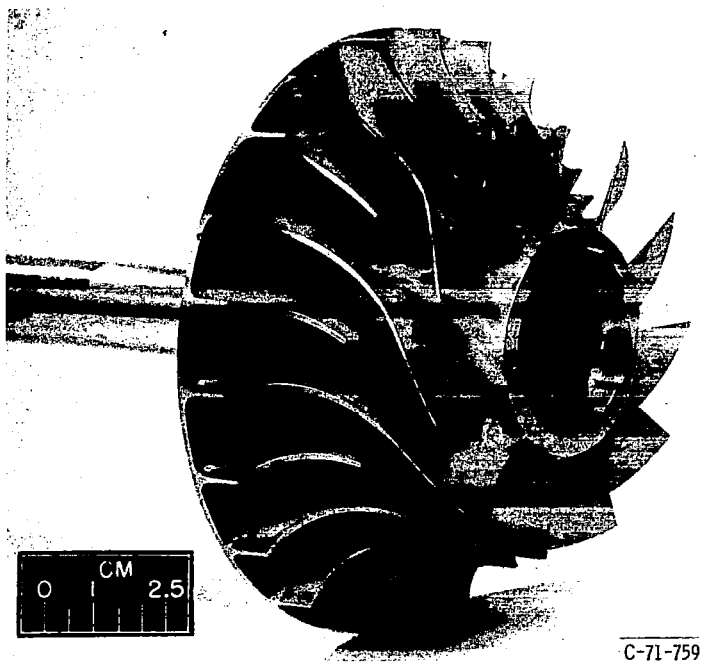


(a) Design rotor.


(b) Rotor with exducer extension.

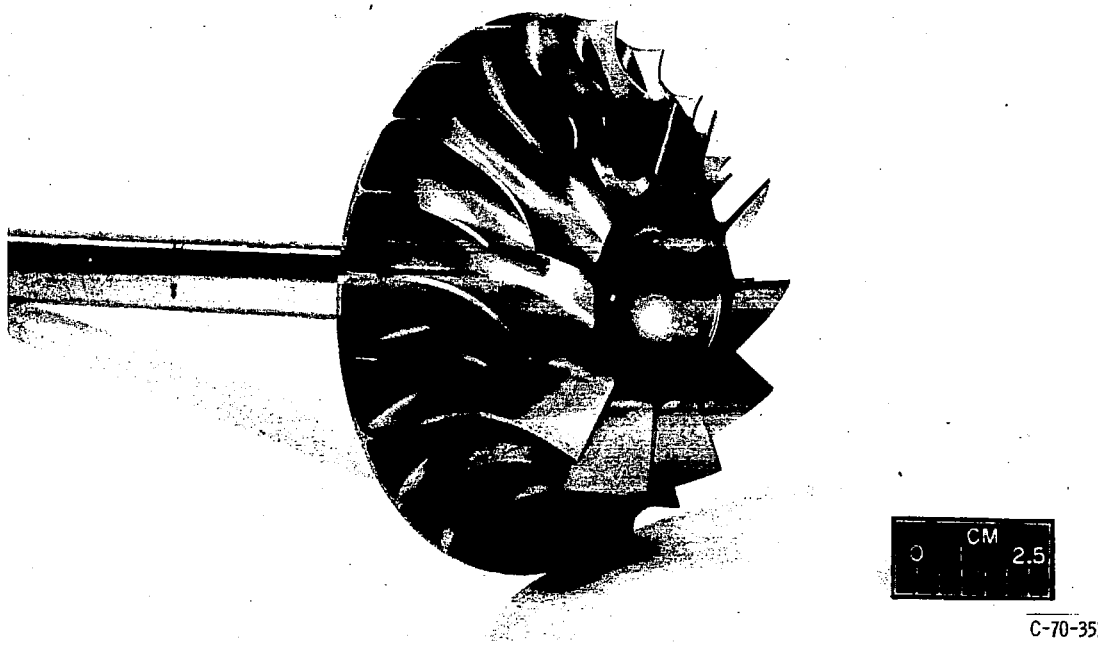


(c) Cutback rotor.

Figure 2. - Rotor configurations investigated.

were completed, the rotor exducer was cut back to provide 137 percent of the design rotor throat area. This rotor configuration would provide a better match of stator and rotor throat areas for the 125- and 144-percent stator configurations.

Figure 1 shows the scroll-stator assembly and a typical stator configuration. The 144-, 125-, and 100-percent stator configurations have 13 blades; the 66-percent stator has 15 blades; and the 42- and 20-percent stators have 17 blades each. Figure 2 shows the design rotor, the exducer extension attached to the rotor, and the rotor with the exducer section cut back. The rotor has 11 blades and 11 splitter vanes. These splitter vanes are used over the initial two-thirds of the design rotor. The splitter vanes were used to prevent low or negative blade-surface velocities, particularly at the rotor hub.

## APPARATUS, INSTRUMENTATION, AND METHODS

The test facility, the instrumentation, and the method of calculating performance parameters were the same as those described in reference 2, except that air was used as the working fluid. Figure 3 shows the turbine test facility. The insulation has been removed from the turbine in order to show details of the test setup. Figure 4 shows a cross-sectional sketch of the turbine test section with the instrument measuring stations. The centerbody was used at the rotor exit in order to obtain measurements of hub static

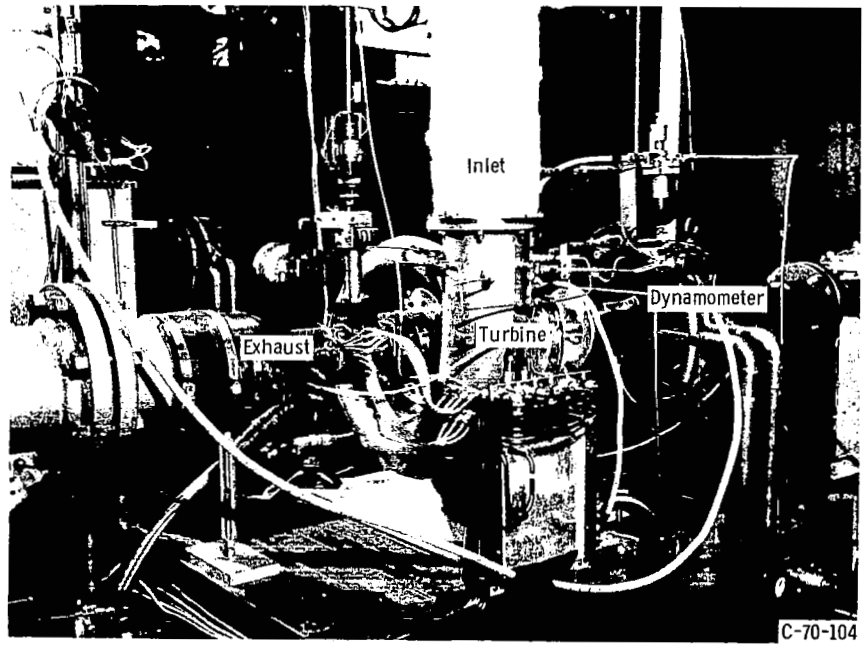


Figure 3. - Turbine test rig.

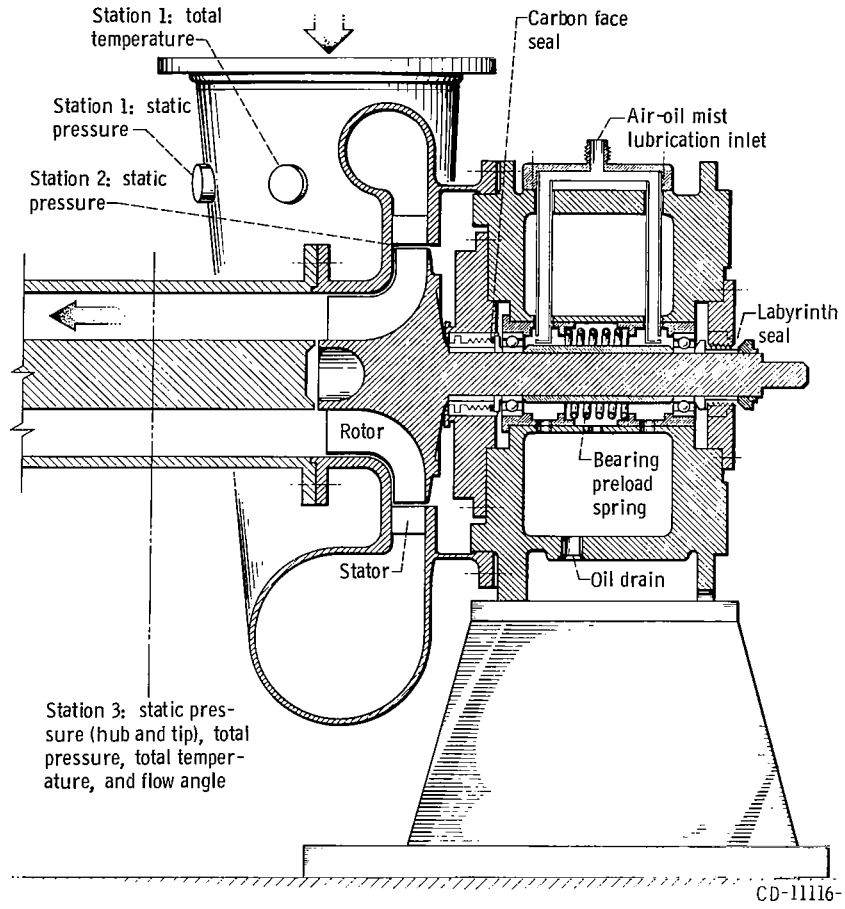


Figure 4. - Turbine instrumentation stations.

pressure and to provide a flow area at the measuring station equal to the flow area at the rotor passage exit. Tip static pressures were also measured at this station. In addition, radial surveys of total pressure, total temperature, and flow angle were made at the rotor exit.

The design or 100-percent stator configuration with design rotor was tested at inlet conditions of 11.0 newtons per square centimeter (16.0 psia) and 306 K (550$^{o}$ R). A mass flow of 0.237 kilogram per second (0.522 lb/sec) was obtained at equivalent design speed and pressure ratio for these inlet conditions. In order to eliminate the effects of changes in Reynolds number on turbine efficiency, this value of mass flow was held approximately constant for all configurations at equivalent design speed and pressure ratio. The inlet total pressure was adjusted until a mass flow of approximately 0.237 kilogram per second (0.522 lb/sec) was obtained. Table I shows the values of inlet total pressure and temperature as well as the pressure ratio range over which the turbine was investigated for each configuration.

TABLE I. - EXPERIMENTAL OPERATING CONDITIONS

| Rotor configuration | Stator configuration, percent of design throat area | Inlet total pressure | | Inlet total temperature | | Pressure-ratio range, $p_1'/p_3$ |
|---|---|---|---|---|---|---|
| | | $N/cm^2$ | psia | K | $^oR$ | |
| Design rotor (design throat area) | 144 | 8.5 | 12.3 | 308 | 555 | 1.40 to 2.16 |
| | 125 | 9.1 | 13.2 | 308 | 555 | 1.40 to 2.12 |
| | 100 | 11.0 | 16.0 | 306 | 550 | 1.41 to 2.13 |
| | 66 | 15.6 | 22.7 | 306 | 551 | 1.41 to 2.12 |
| | 42 | 21.9 | 31.8 | 306 | 551 | 1.46 to 2.05 |
| | 20 | 40.3 | 58.4 | 306 | 550 | 1.55 to 2.12 |
| With exducer extension (53 percent of design throat area) | 100 | 13.7 | 19.9 | 305 | 549 | 1.40 to 2.25 |
| | 66 | 17.4 | 25.2 | 304 | 548 | 1.41 to 2.16 |
| | 42 | 24.6 | 35.7 | 305 | 549 | 1.41 to 2.10 |
| | 20 | 41.6 | 60.3 | 305 | 549 | 1.53 to 2.19 |
| Cutback rotor (137 percent of design throat area) | 144 | 7.8 | 11.3 | 306 | 550 | 1.40 to 2.09 |
| | 125 | 8.7 | 12.7 | 305 | 549 | 1.40 to 2.09 |
| | 100 | 10.0 | 14.5 | 306 | 550 | 1.39 to 2.10 |

Thus, the effect of specific speed variation was evaluated at constant Reynolds number. Reynolds number as defined in this report is equal to the mass flow divided by the product of the gas viscosity and the rotor inlet tip radius. Mass flow would be varied in order to operate at different power levels in the actual space-power package. The Reynolds number effects, for this type of operation, could be calculated using figure 14 of reference 2.

## RESULTS AND DISCUSSION

Performance results are presented in four sections. The first section describes the results that were obtained by using the rotor as it was designed with the six stators of different throat areas. The second section shows the results that were obtained by using the rotor with the extension and four stator configurations (100, 66, 42, and 20 percent of design throat area). The third section shows the results that were obtained with the cutback rotor and with the 100-, 125-, and 144-percent stator configurations. All data presented are for operation at equivalent design speed and with cold air as the working fluid. The performance data are shown in terms of equivalent mass flow for a range of pressure ratios and turbine efficiency over the range of specific speed. There follows a discussion of the internal flow characteristics as determined from radial surveys of angle, total pressure, and total temperature that were made at the rotor exit and the static pressure measurements throughout the turbine. The fourth section then compares efficiency as a function of specific speed for the three rotor configurations in order to determine the stator-rotor combinations that give the highest efficiencies at various specific speeds.

Results of an analysis made to determine the magnitude of the various turbine losses for each stator-rotor combination are shown in appendix B. Velocity diagrams and blade-surface velocities for each stator-rotor combination are presented and discussed in appendixes C and D, respectively.

### Performance with Design Rotor

Mass flow. - Figure 5 shows the variation of equivalent mass flow $\epsilon w\sqrt{\theta_{cr}}/\delta$ with equivalent inlet-total to exit-static pressure ratio $(p_1'/p_3)_{eq}$. Equivalent mass flow increased with an increase in pressure ratio for all stator configurations. This variation in mass flow with pressure ratio indicates subsonic flow over the range of pressure ratios covered. It can be seen that the slope of the curves decreases with a decrease in stator throat area. The slope of the curve for the 20-percent configuration is near

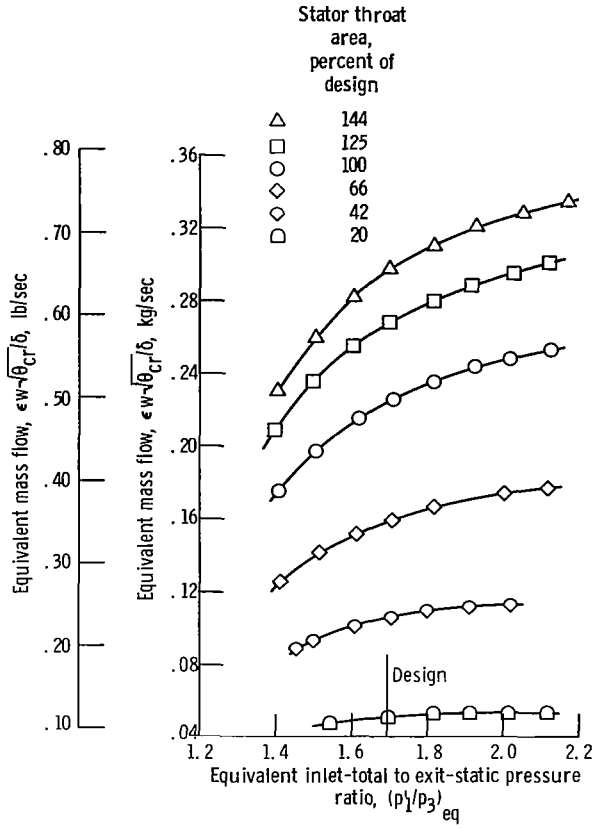


Figure 5. - Variation of equivalent mass flow with pressure ratio and stator throat area at equivalent design speed; design rotor.

zero at pressure ratios greater than 2.0. In this region of operation, a near-choked flow condition exists. Equivalent mass flows of 0.050, 0.105, 0.158, 0.224, 0.267, and 0.297 kilogram per second (0.111, 0.231, 0.348, 0.494, 0.589, and 0.655 lb/sec) were obtained for the 20-, 42-, 66-, 100-, 125-, and 144-percent configurations, respectively, at an equivalent design pressure ratio of 1.695. The mass flow for the 100-percent configuration was about 1.6 percent larger than the design value of 0.2204 kilogram per second (0.486 lb/sec).

Figure 6 shows the effect of the change in stator throat area on stator-exit static pressure. As stator throat area is increased, there is an increase in the stator pressure ratio $p_2/p'_1$. This increase in stator pressure ratio results in a decrease in velocity level through the stator and will, therefore, have an effect on the mass flow rate. The figure also shows that rotor reaction increased with increasing stator throat area.

Figure 7 shows mass flow as a function of stator throat area. The mass flow obtained for each stator configuration at equivalent design pressure ratio (1.695) is expressed as a percentage of the mass flow obtained with the 100-percent configuration.

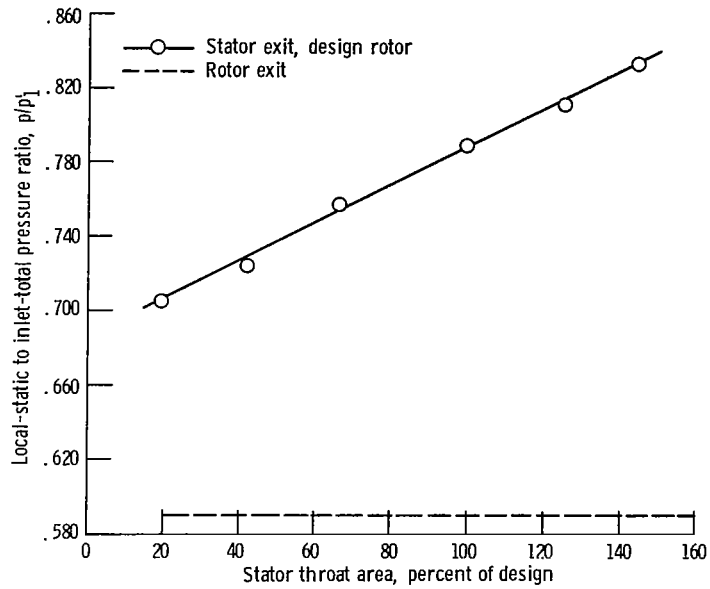


Figure 6. - Variation of stator-exit static pressure with stator throat area at equivalent design speed and pressure ratio; design rotor.

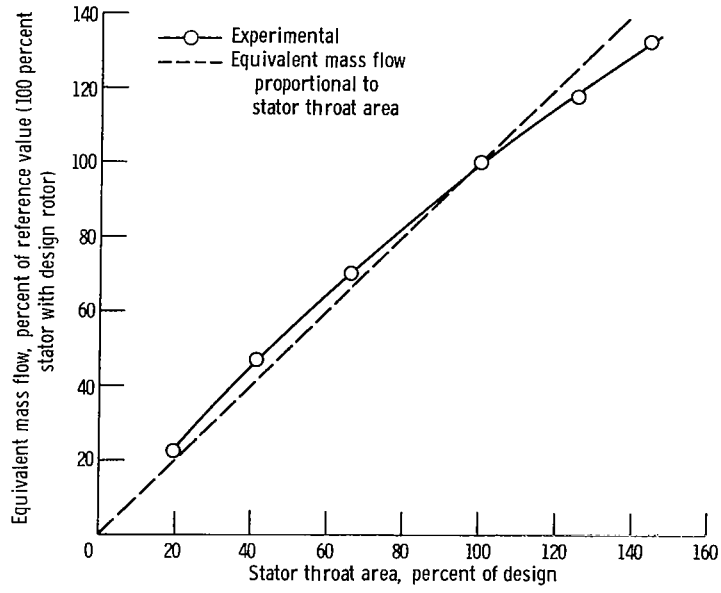


Figure 7. - Variation of equivalent mass flow with stator throat area at equivalent design speed and pressure ratio; design rotor.

The dashed line in the figure represents an equivalent mass flow that is directly proportional to the stator throat area. There is a difference in the slopes of the two lines. The difference in mass flow variation is due to the previously shown change in stator-exit static pressure with the change in stator throat area. Calculated mass flows based on the measured static pressures and a constant total pressure agreed with the measured mass flow. This indicates that there was no measurable change in loss upstream of the stator throat and that the mass flow was affected only by the change in stator throat area and pressure ratio.

Efficiency. - Figure 8 shows the variations of total and static efficiencies with specific speed for each of the six stator configurations. Use of the six stators resulted in covering a specific speed range from 0.25 to 0.77 (32 to 99). The short-dashed line shows the variation of efficiency with specific speed at the design blade-jet speed ratio of 0.690. The heavy line is the envelope of the efficiency curves for all configurations. A peak total efficiency of 0.925 (fig. 8(a)) was obtained for both the 66-percent and the 100-percent configurations. The figure shows that a total efficiency value of 0.90 or higher could be obtained over a specific speed range of 0.43 to 0.71 (55 to 91). The figure also shows that the design blade-jet speed ratio curve passes through the peak efficiency point for the 100-, 125-, and 144-percent stator configurations. As the stator throat area is decreased, the peak efficiency points continue to shift to lower values of blade-jet speed ratio. This shift indicates that optimum velocity diagrams were not

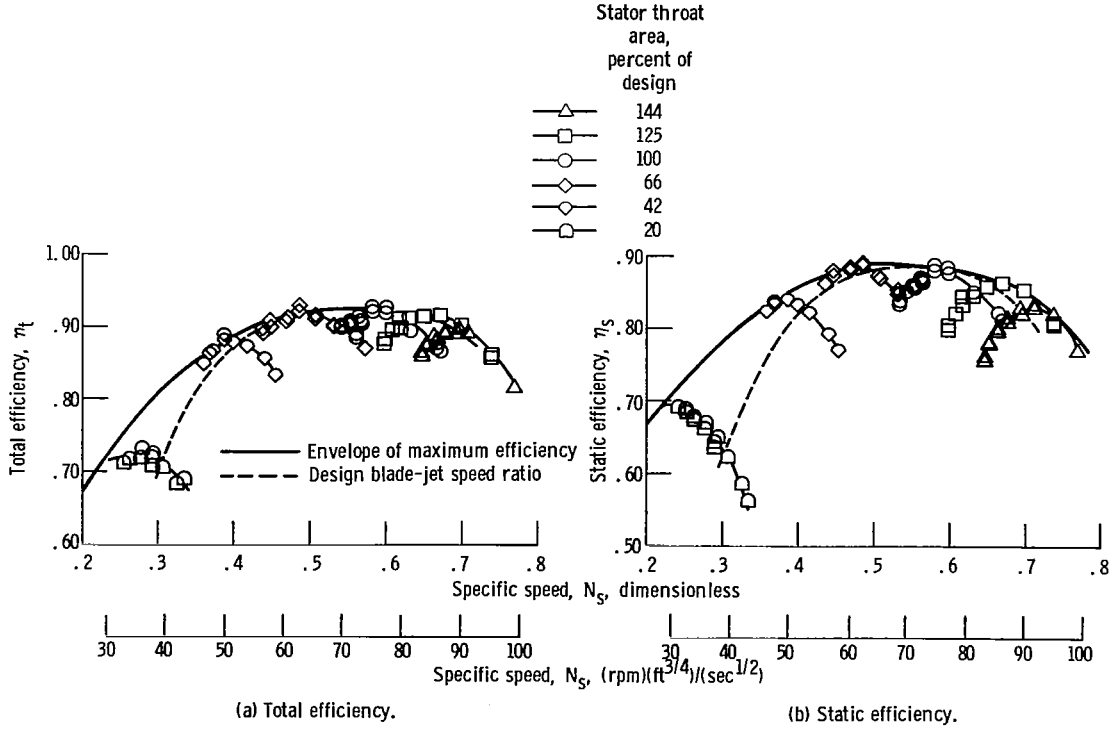


Figure 8. - Variation of efficiency with specific speed at equivalent design speed; design rotor.

obtained at design blade-jet speed ratio. It should be noted that the design rotor was used with each stator for this series of tests. The end result was an increasing mismatch between stator and rotor throat areas as the stator throat areas were reduced. The mismatch also increased progressively with the oversized stator configurations.

Figure 8(b) shows the variation of static efficiency with specific speed. Both the 66-percent and the 100-percent stator configurations gave a peak efficiency value near 0.88. The heavy solid line curve shows that a maximum value of 0.89 could be obtained at a specific speed of about 0.51 (66). There is a rapid decrease in efficiency at both ends of the specific speed curve. The peak efficiency point shifts to lower values of blade-jet speed ratio as the specific speed is decreased from the 100-percent stator configuration.

Internal flow characteristics. - The results of a radial survey of exit flow angle taken at equivalent design speed and pressure ratio are shown in figure 9. As stator throat area was reduced, the exit flow angle became more positive over the entire passage height. This trend in exit flow angle with stator configuration is to be expected since the rotor exit relative velocity decreases with decreasing stator throat area as seen from the velocity diagrams of appendix C.

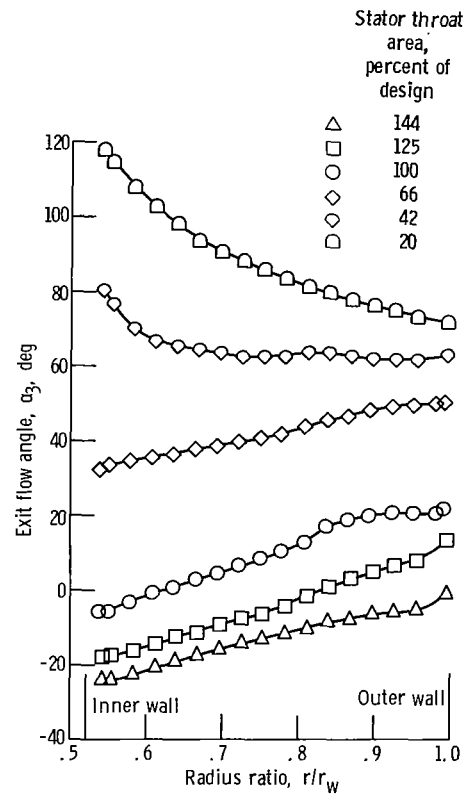


Figure 9. - Variation of exit flow angle with radius ratio at equivalent design speed and pressure ratio; design rotor.

For the 20-percent stator configuration, exit flow angles greater than $90^{o}$ from axial were obtained from the hub to a radius ratio of 0.70. A one-dimensional calculation of mass flow using the results of the survey did not agree with the measured mass flow for the 20-percent stator. This indicates that either the flow angle measurements were incorrect or that a one-dimensional flow solution was inadequate for this stator-rotor combination. Figure 26 of appendix D shows calculated rotor blade surface velocities for all stator-rotor configurations investigated. The figure shows negative pressure surface velocities for the hub, mean, and tip sections when the 20-percent stator was used with the design rotor. Negative pressure surface velocities, especially at the inlet portion of the blade, could have resulted in flow eddy. It would appear that the angle measurements for the 20-percent stator configuration were not correct and that the radius ratio at which flow angles greater than $90^{o}$ were obtained were nearer the hub section than is shown by the figure.

The results of a radial survey of rotor exit flow angle, total pressure, and temperature are shown in figure 10 as a variation of turbine loss with radius ratio. Turbine loss

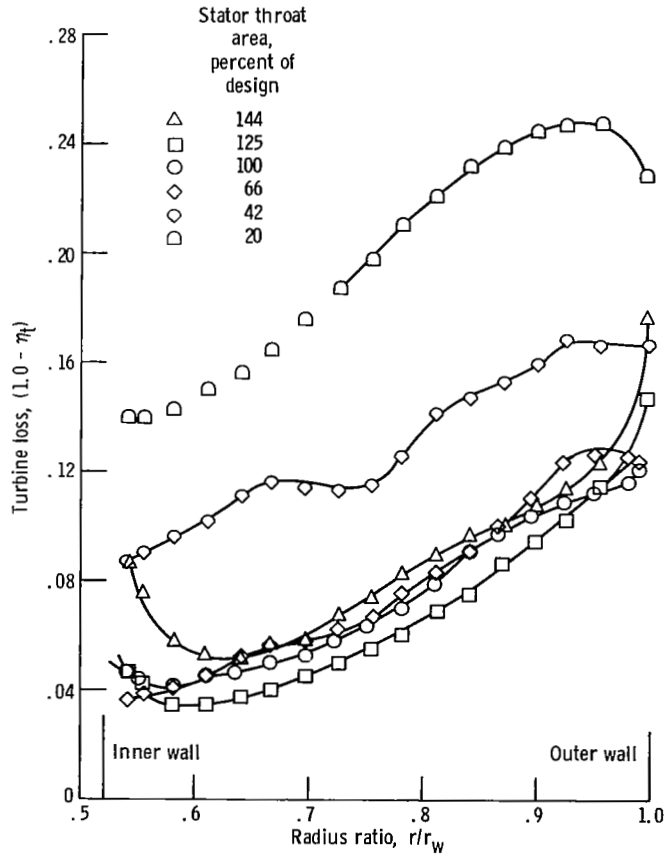


Figure 10. - Variation of turbine loss with radius ratio at equivalent design speed and pressure ratio; design rotor.

is defined as 1.0 minus the local total efficiency. The curve for the 20-percent stator configuration does not have a faired line for the radius ratio range of 0.52 to 0.72 because the inlet tangential momentum could not be computed accurately since exit flow angles greater than $90^{\circ}$ were obtained in this region. The figure shows comparable losses for the 66-, 100-, 125-, and 144-percent stator configurations. This was to be expected since the turbine efficiency was about the same at equivalent design speed and pressure ratio. The losses for the 20- and 42-percent stator configurations were large over the entire passage height. Maximum losses were obtained in the tip region for all configurations.

## Performance with Rotor Extension

Mass flow. - Figure 11 shows the variation of equivalent mass flow $\epsilon w\sqrt{\theta_{cr}}/\delta$ with equivalent inlet-total to exit-static pressure ratio $(p_1'/p_3)_{eq}$. The shapes of the curves obtained with the rotor extension are similar to those obtained with the design rotor (fig. 5). There is a difference, however, in the level of the curves for the two cases. The rotor throat area was reduced to 53 percent of the design value with the addition of the rotor extension. This resulted in a reduction in equivalent mass flow for the three larger area stators. There was no change for the stator with the 20-percent throat area since it was operating near the choked condition (as shown by the slope of the mass flow curve in fig. 5).

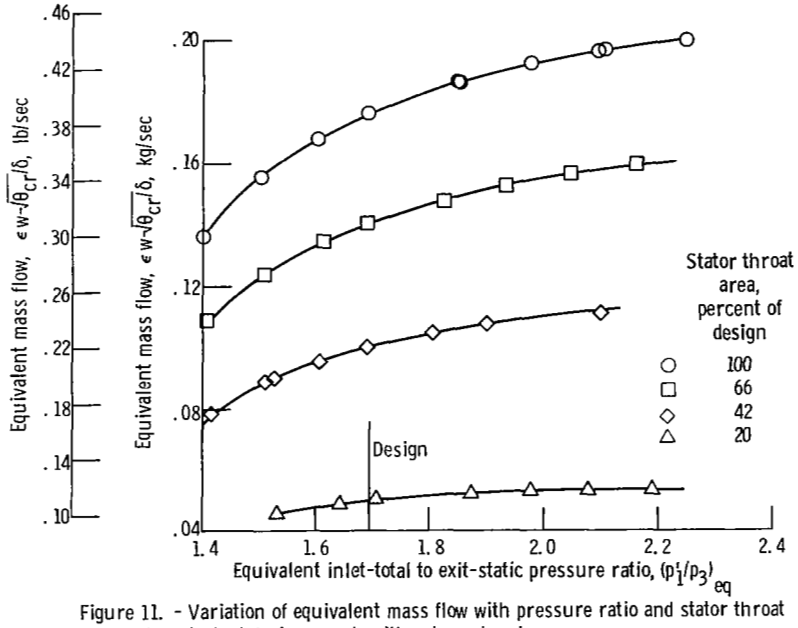


Figure 11. - Variation of equivalent mass flow with pressure ratio and stator throat area at equivalent design speed; with rotor extension.

The variation of stator-exit static pressure with a change in stator throat area is shown in figure 12 for operation with the rotor extension. The static-pressure variation for operation with the design rotor is also shown for comparison. The stator-exit pressure with the extended rotor is greater than that for the design rotor. There was, therefore, a decrease in velocity level through the stator and an associated decrease in mass flow rate when compared with the results obtained with the design rotor. Rotor reaction is larger over the entire stator throat area range for the case with the rotor extension.

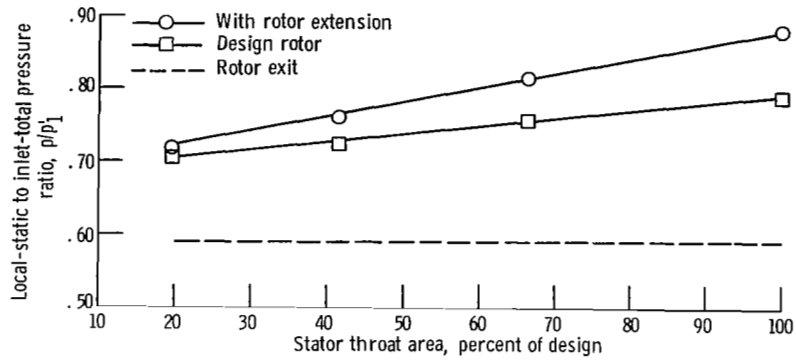


Figure 12. - Variation of stator-exit static pressure with stator throat area at equivalent design speed and pressure ratio; with rotor extension.

Figure 13 shows the variation of equivalent mass flow with stator throat area for operation at equivalent design speed and pressure ratio. Mass flow is expressed as a percent of that obtained with the 100-percent stator throat area and with the design rotor. The dashed line represents an equivalent mass flow that is directly proportional to the stator throat area. The difference between the dashed and experimental curves is due to the stator-exit static pressure variation indicated in figure 12. The experimental curve intersects the dashed curve at a stator throat area value of about 57 percent of design. This indicates that design velocities as well as design rotor reaction would be obtained in this region.

Efficiency. - Figure 14 shows the variations of total and static efficiencies with specific speed for each of the four stator configurations. The short-dashed line represents operation at the design blade-jet speed ratio of 0.690. The heavy curve is the envelope of the efficiency curves for all configurations. A peak value of total efficiency (fig. 14(a)) of 0.92 was obtained with the 66-percent stator configuration at a specific speed of 0.45 (58.0). The heavy curve shows a maximum total efficiency of 0.925 at a specific speed of about 0.43 (55.4). The value of about 0.92 or higher can be obtained within the specific speed range of about 0.41 to 0.46 (53 to 59). Variation from this range

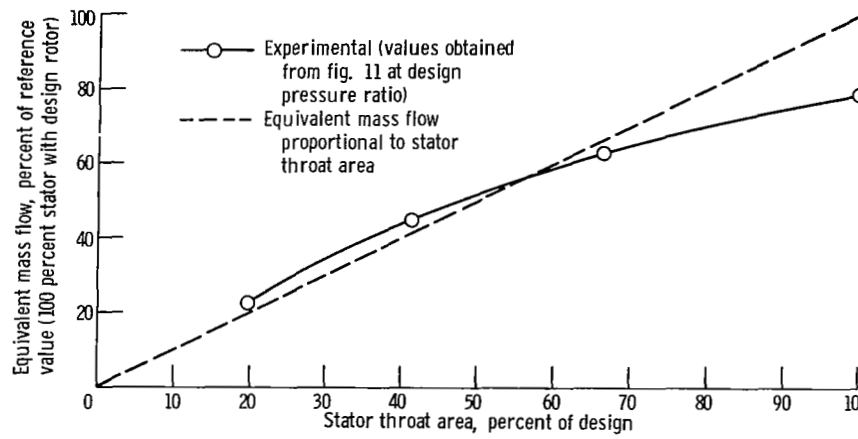


Figure 13. - Variation of equivalent mass flow with stator throat area at equivalent design speed and pressure ratio; with rotor extension.

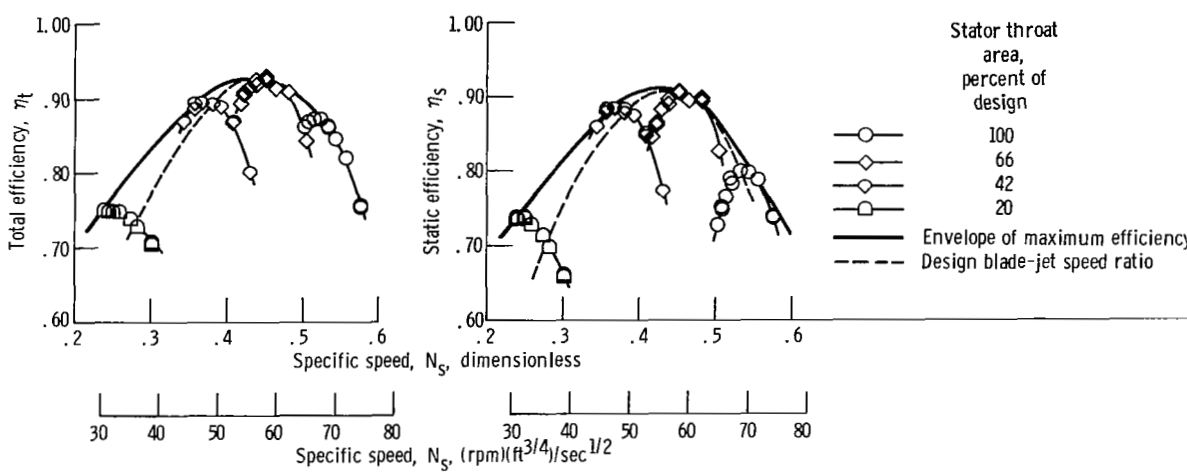


(a) Total efficiency.

(b) Static efficiency.

Figure 14. - Variation of efficiency with specific speed at equivalent design speed; with rotor extension.

results in a rapid decrease in efficiency. A peak value of static efficiency of 0.90 (fig. 14(b)) was obtained with the 66-percent stator at a specific speed of about 0.45 (58). The heavy curve shows that the maximum static efficiency of 0.91 falls within the same specific speed range of 0.41 to 0.46 (53 to 59).

Internal flow characteristics. - The results of a radial survey of exit flow angle taken at equivalent design speed and pressure ratio are shown in figure 15. As stator throat area was reduced, the exit flow angle became more positive over the entire passage height. This trend in exit flow angle with stator configuration is to be expected because the rotor exit relative velocity decreases with decreasing stator throat area as seen from the velocity diagrams of appendix C.

For the 20-percent stator configuration, exit flow angles greater than $90^{o}$ were obtained from the hub to a radius ratio of 0.630. One-dimensional calculations of mass flow, using the results of the survey, were in good agreement with the measured mass flow for the 20-percent stator with the rotor extension. This would indicate that the

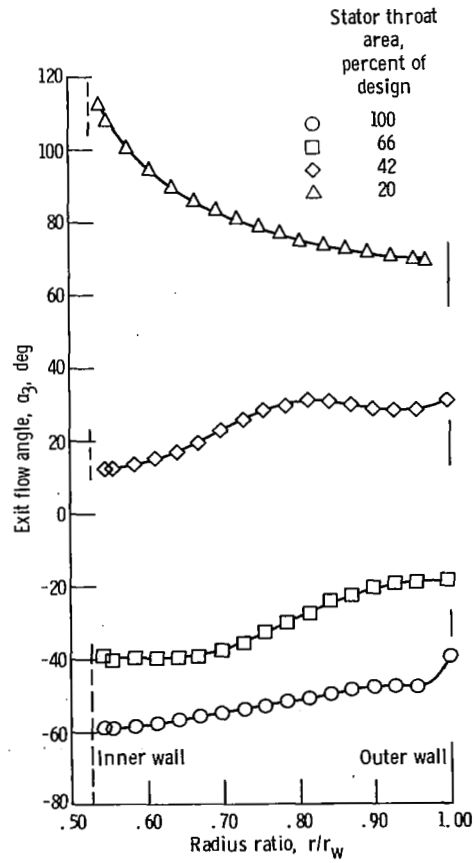


Figure 15. - Variation of exit flow angle with radius ratio at equivalent design speed and pressure ratio; with rotor extension.

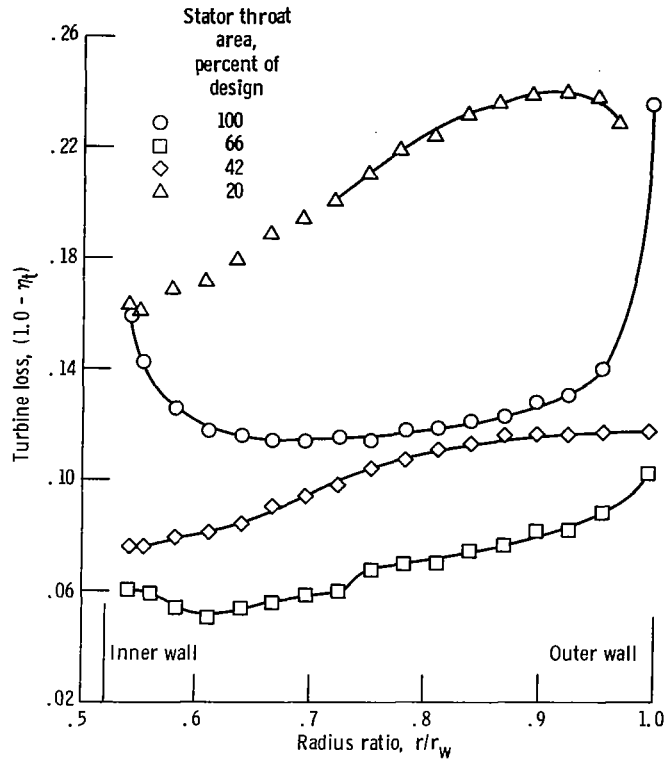


Figure 16. - Variation of turbine loss with radius ratio at equivalent design speed and pressure ratio; with rotor extension.

rotor flow angle measurements were good for this survey. Figure 27, appendix D, shows that there was considerable negative rotor surface velocities for the 20-percent stator with the rotor extension. Negative suction surface velocities occurred on the hub and mean sections of the rotor blade. Considerable suction surface deceleration occurred at the hub section. This could result in the flow separation indicated by the angle survey.

The variation of exit flow angle and exit total and static pressure with radius ratio indicated that there was a nonuniform work distribution from hub to outer wall for all configurations.

Turbine loss ($1.0-\eta_t$) as a function of radius ratio is shown in figure 16. The loss data were not faired for the radius ratio range of 0.52 to 0.72 for the 20-percent configuration because of the possible flow separation and backflow in this region. Except for the 100-percent stator configuration, the losses were lowest near the hub region and increased with increasing radius ratio.

## Performance with Cutback Rotor

Mass flow. - Figure 17 shows the variation of equivalent mass flow $\epsilon w\sqrt{\theta_{cr}}/\delta$ with equivalent inlet total to exit static pressure ratio $(p_1'/p_3)_{eq}$. The shapes of the curves obtained with the cutback rotor are similar to those obtained with the design rotor (fig. 5). The difference is in the magnitude of the mass flow between the two cases. The rotor throat area was increased to 137 percent of the design value. There was, therefore, an increase in mass flow for the three stator configurations investigated with the cutback rotor.

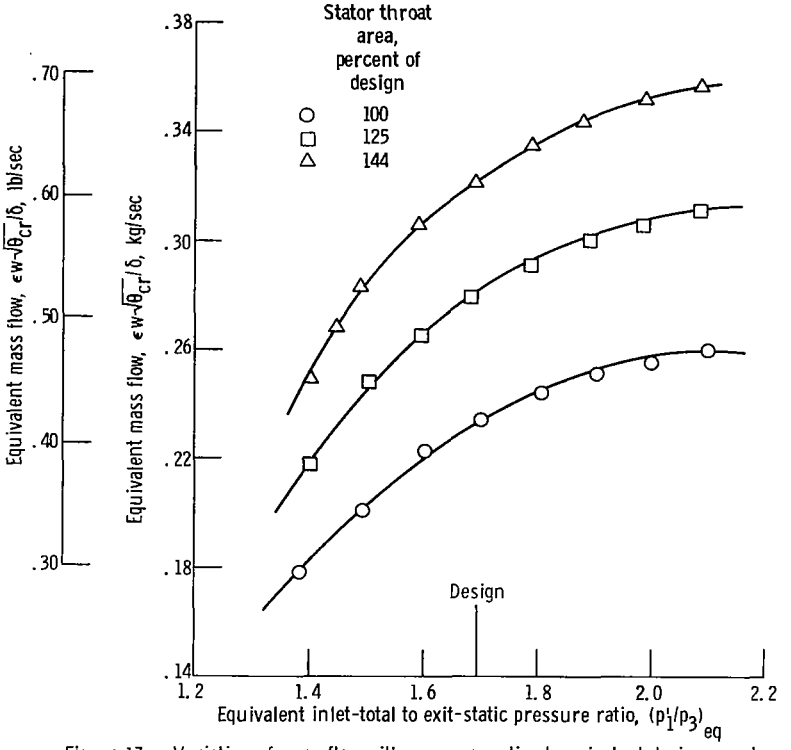


Figure 17. - Variation of mass flow with pressure ratio at equivalent design speed; cutback rotor.

Figure 18 shows the change of stator-exit static pressure with percent stator throat area at equivalent design speed and pressure ratio. Stator exit velocity decreases and rotor reaction increases with increasing stator throat area. The solid curve from figure 7, shows the variation of stator-exit static pressure with percent stator throat area for the tests with the design rotor configuration. Rotor reaction is smaller over the entire stator throat area range for the case with the cutback rotor. This is to be expected because the larger rotor throat area would require a greater flow rate (at a

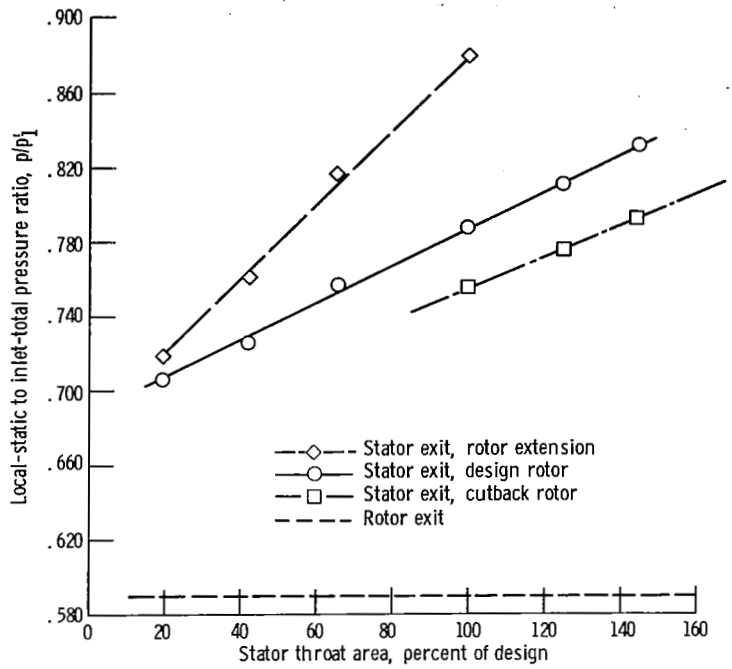


Figure 18. - Variation of stator-exit static pressure with stator throat area at equivalent design speed and pressure ratio; cutback rotor.

given turbine inlet pressure) to obtain equivalent design speed and pressure ratio. The higher flow rate is reflected in the lower stator-exit static pressure for the data obtained with the cutback rotor. The figure shows that the combination of the 137-percent stator area configuration with the cutback rotor would be required to give approximately the same rotor reaction as that obtained with the 100-percent stator configuration and the design rotor. This is to be expected since the cutback rotor was 137 percent of design rotor throat area. The long-dashed curve from figure 12 shows the variation of stator-exit static pressure with percent stator throat area for the tests with the rotor extension. Comparison of the static pressure for the three rotor configurations shows that the stator-exit velocity was the lowest for the rotor extension configuration over the range of stator throat areas investigated. The figure also shows that design velocity diagrams would be obtained with a 53-percent stator throat area and the rotor extension as well as with a 137-percent stator throat area with the cutback rotor.

Figure 19 shows the variation of equivalent mass flow with stator throat area for operation at equivalent design speed and pressure ratio. Mass flow is expressed as a percent of that obtained with the 100-percent stator throat area and with the design rotor. The dashed line represents an equivalent mass flow that is directly proportional to the stator throat area. The difference between the dashed and experimental curves is due to the stator-exit static pressure variation indicated in figure 18. Figure 19 shows that the experimental curve intersects the dashed curve at a stator throat area value of about

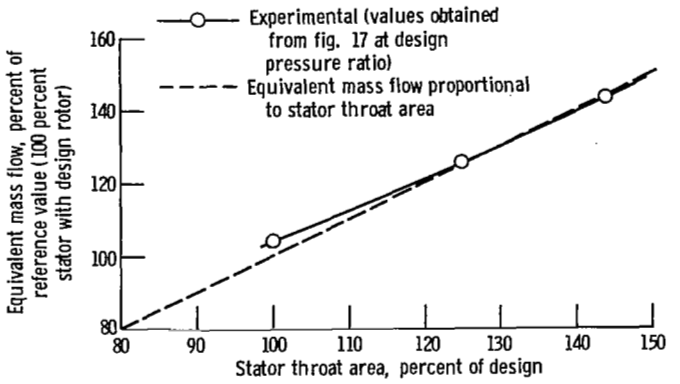


Figure 19. - Variation of equivalent mass flow with stator throat area at equivalent design speed and pressure ratio; cutback rotor.

130 to 135 percent of design. This indicates that design velocities and approximately design rotor reaction would be obtained in this region.

Efficiency. - Figure 20 shows the variations of total and static efficiencies with specific speed for each of the three stator configurations. The heavy curve is the envelope of the efficiency curves for the three configurations. The short-dashed curve represents operation at design blade-jet speed ratio of 0.690. Figure 20(a) shows total efficiency as a function of specific speed. Design blade-jet speed ratio points are on the envelope curve. The figure shows that a peak efficiency of 0.915 is obtained for the 125- and 144-percent configurations. This is slightly higher than that obtained with the 100-percent configuration. The main point that the figure shows is that the envelope

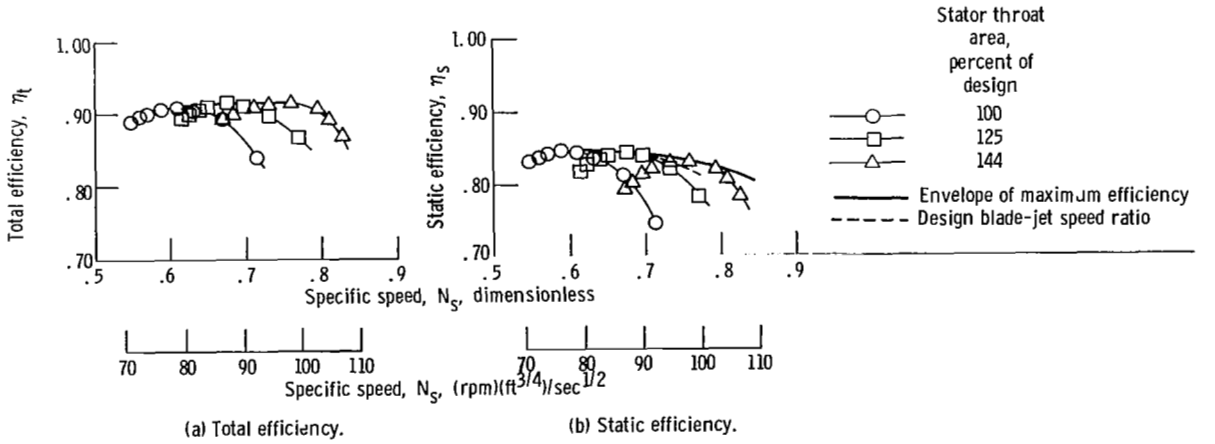


(a) Total efficiency. (b) Static efficiency.

Figure 20. - Variation of efficiency with specific speed at equivalent design speed; cutback rotor.

curve is flat and that total efficiencies of 0.90 and greater can be obtained over a specific speed range of 0.57 (73) to 0.80 (102).

Figure 20(b) shows the variation of static efficiency with specific speed. The figure shows that the peak efficiency decreases with increasing stator throat area. This results from the increasing rotor exit velocity as a result of the increasing mass flow with increasing stator throat area. The figure shows that peak static efficiencies of 0.845, 0.840, and 0.830 were obtained with the 100-, 125-, and 144-percent stator configurations, respectively.

Internal flow characteristics. - Figure 21 shows the variation of rotor exit flow angle with radius ratio. The figure shows that as the stator throat area was increased, the exit flow angle became less positive. This results from the increased rotor relative velocity through the rotor with increasing stator throat area. The wheel speed was constant for all configurations investigated.

Figure 22 shows the variation of turbine loss with radius ratio for the three stator configurations. The data were obtained at equivalent design speed and pressure ratio. Local values of total efficiency were calculated on the basis of the change in tangential momentum through the rotor and the radial distribution of total pressure at the rotor exit. The figure shows that minimum losses were obtained with the 144-percent stator configuration. The largest losses were obtained with the 100-percent stator configuration. This was to be expected as the total efficiency plot of figure 20(a) indicated in-

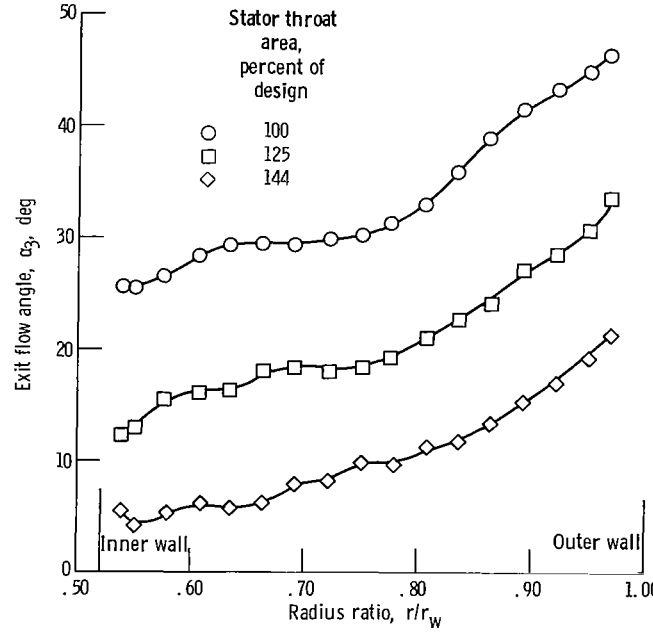


Figure 21. - Variation of exit flow angle with radius ratio at equivalent design speed and pressure ratio; cutback rotor.

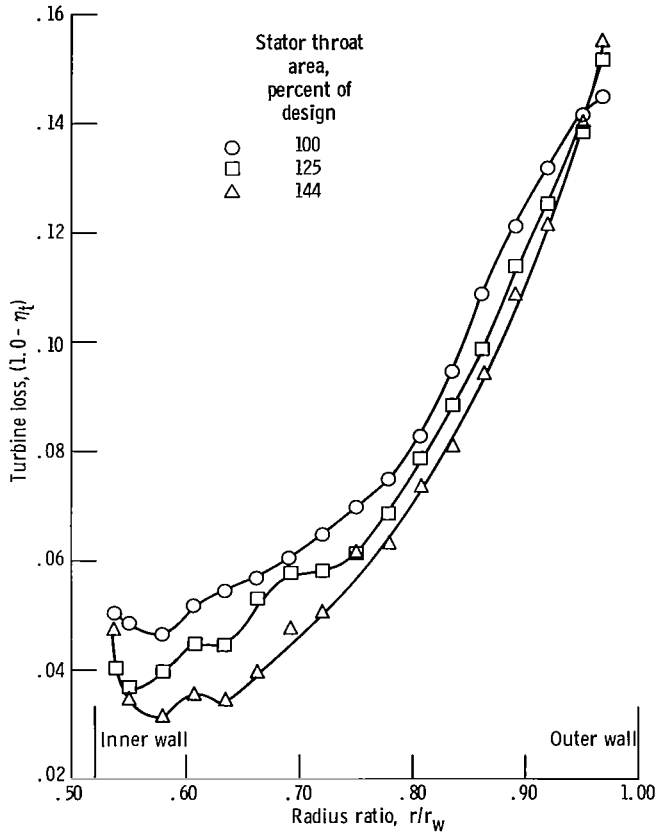


Figure 22. - Variation of turbine loss with radius ratio at equivalent design speed and pressure ratio; cutback rotor.

creased efficiency with increasing stator throat area. The figure also shows minimum losses near the hub region with the losses increasing with increasing radius ratios for the three stator configurations investigated.

## Comparison of Efficiencies for the Three Rotors

A comparison of the performance of the turbine with the rotor configurations investigated is best shown by replotting some of the curves already presented. The total efficiency envelope curves of figures 8(a), 14(a), and 20(a) are shown in figure 23(a). In addition, the envelope of these three curves is also shown. A maximum total efficiency of 0.925 is obtained over the wide range of specific speeds from 0.42 to about 0.65 (55 to 85). The figure also shows that total efficiencies of 0.90 and greater can be obtained over the large specific speed range of 0.37 to 0.80 (48 to 104). The figure indicates a slight decrease in performance in the high specific speed range (above 0.70 (91)). It is to be expected that the efficiency would drop off more rapidly in the specific speed range below 0.40 (52). In this lower range, excessive stator losses due to trailing edge blockage would cause the rapid decrease in turbine efficiency.

The figure also shows that the same maximum total efficiency of 0.925 is obtained for the design rotor and the rotor with the exducer extension. Operation with the cutback rotor resulted in only about one point drop in maximum total efficiency.

Figure 23(b) shows the comparison between maximum static efficiencies for operation with the rotor configurations investigated. These curves are the envelope curves of figures 8(b), 14(b), and 20(b). The envelope of these curves is also shown. A max-

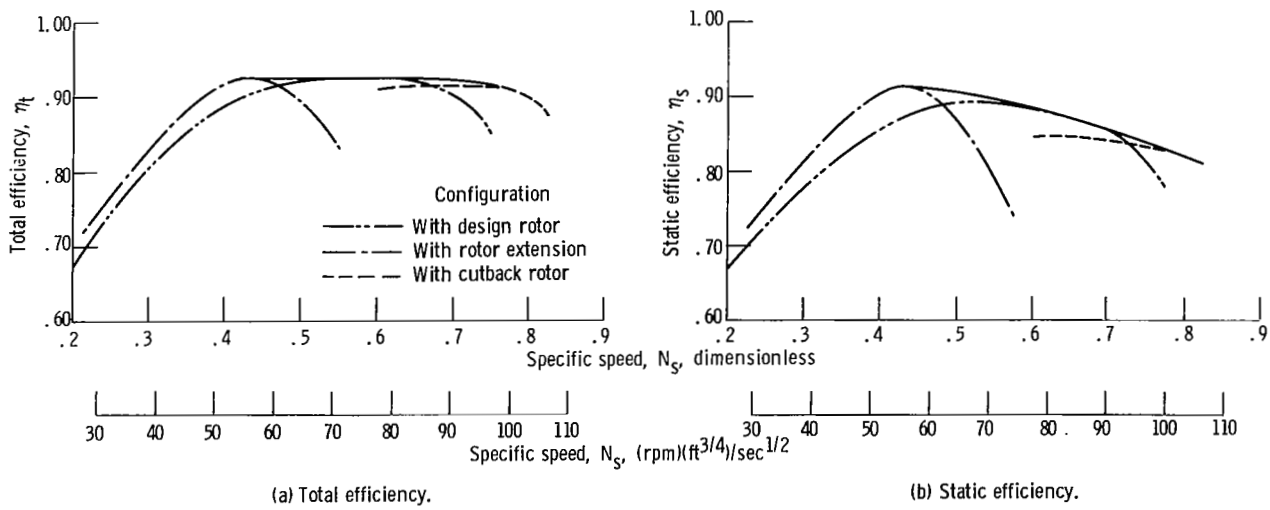


Figure 23. - Variation of efficiency with specific speed at equivalent design speed with best stator-rotor combination.

TABLE II. - STATOR-ROTOR COMBINATIONS FOR MAXIMUM EFFICIENCY

| Rotor configuration | Stator configuration, percent of design throat area | Maximum total efficiency | Specific speed at maximum total efficiency | | Maximum static efficiency | Specific speed at maximum static efficiency | |
|---|---|---|---|---|---|---|---|
| | | | Dimensionless | $(rpm)(ft^{3/4})/sec^{1/2}$ | | Dimensionless | $(rpm)(ft^{3/4})/sec^{1/2}$ |
| Design rotor (design throat area) | 66 | 0.925 | 0.49 | 63.2 | 0.880 | 0.48 | 61.9 |
| | 100 | .925 | .60 | 77.4 | .880 | .59 | 76.1 |
| With exducer extension (53 percent of design throat area) | 66 | 0.920 | 0.45 | 58.0 | 0.900 | 0.45 | 58.0 |
| Cutback rotor (137 percent of design throat area) | 100 | ----- | ---- | ---- | 0.845 | 0.59 | 76.1 |
| | 125 | 0.915 | 0.67 | 86.4 | ----- | ---- | ---- |
| | 144 | .915 | .76 | 98.0 | ----- | ---- | ---- |

imum static efficiency of 0.91 is obtained at a specific speed value of about 0.43 (56). The figure also shows that the maximum static efficiency was obtained with the rotor extension. The higher static efficiency results from a lower exit kinetic energy level for operation with the rotor extension when compared with that obtained with the design and cutback rotor configurations. The figure also shows that a static efficiency of 0.85 and greater can be obtained over a large specific speed range of 0.34 to 0.72 (44 to 94). The decrease in static efficiency with increasing specific speed results from the increasing rotor exit kinetic energy level with increasing specific speed.

Table II lists the stator-rotor combinations that gave the maximum static and total efficiencies for the specific speed range investigated. Figure 23 and table II indicate that, if high efficiency is desired over a wide range of specific speeds, optimum stator-rotor throat area ratio should be maintained when stator throat area is changed.

## SUMMARY OF RESULTS

An experimental cold-air investigation was made to determine the effect of specific speed on the performance of a 12.62-centimeter (4.97-in.) tip diameter radial-inflow turbine. The range of specific speed values was obtained by changing volume flow through the turbine by changing stator throat area. Tests were made with stator throat areas of 20, 42, 66, 100, 125, and 144 percent of design with the design rotor. In addition, a rotor exducer extension that reduced rotor throat area to 53 percent of design and a cutback rotor configuration that increased rotor throat area to 137 percent of design were used with some of the stator configurations. Results are presented for operation with the 13 combinations of stator and rotor configurations at equivalent design speed and over a range of pressure ratios. These results can be summarized as follows:

1. Results using the best stator-rotor configurations investigated showed that total efficiencies of 0.90 and greater can be obtained over a large specific speed range of 0.37 to 0.80 (48 to 104). Similarly, static efficiencies of 0.85 and greater can be obtained over the comparatively large specific speed range of 0.34 to 0.72 (44 to 94).

2. A maximum total efficiency of 0.925 was obtained over the specific speed range of 0.42 to 0.65 (55 to 85). The maximum static efficiency of 0.91 was obtained at a specific speed of 0.43 (56).

3. If high efficiency is desired over a large range of specific speeds, optimum stator-rotor throat area ratio should be maintained when stator throat area is changed.

4. Rotor exit flow angle surveys indicated possible flow separation in the rotor hub region when operated with the 20-percent stator configuration. This was substantiated by calculated rotor-blade-surface velocities, which indicated negative pressure surface velocities and considerable flow deceleration.

Lewis Research Center,
National Aeronautics and Space Administration,
Cleveland, Ohio, September 17, 1971,
112-27.

# APPENDIX A

## SYMBOLS

$H'$ isentropic specific work (based on total pressure ratio), J/g; ft-lb/lb

$\Delta h$ specific work, J/g; Btu/lb

$N$ turbine speed, rpm

$N_s$ specific speed, $NQ^{1/2}/(H')^{3/4}$, dimensionless; rpm $(ft^{3/4})/(sec^{1/2})$

$p$ pressure, $N/cm^2$ abs; psia

$Q$ volume flow (based on exit conditions), $m^3/sec$; $ft^3/sec$

$Re$ Reynolds number, $w/\mu r_t$

$r$ radius, m; ft

$U$ blade velocity, m/sec; ft/sec

$V$ absolute gas velocity, m/sec; ft/sec

$V_j$ ideal jet speed corresponding to total- to static-pressure ratio across turbine, m/sec; ft/sec

$w$ weight flow, kg/sec; lb/sec

$\alpha$ absolute gas flow angle measured from axial direction, deg

$\gamma$ ratio of specific heats

$\delta$ ratio of inlet total pressure to U.S. standard sea-level pressure $p_1'/p^*$

$\epsilon$ function of $\gamma$ used in relating parameters to those using air inlet conditions at U.S. standard sea-level conditions, $\frac{0.740}{\gamma}\left[\left(\frac{\gamma+1}{2}\right)\right]^{\gamma/(\gamma-1)}$

$\eta$ turbine efficiency

$\eta_s$ static efficiency (based on inlet-total- to exit-static-pressure ratio)

$\eta_t$ total efficiency (based on inlet-total- to exit-total-pressure ratio)

$\theta_{cr}$ squared ratio of critical velocity at turbine inlet to critical velocity at U.S. standard sea-level temperature, $(V_{cr}/V_{cr}^*)^2$

$\mu$ gas viscosity, kg/(m)(sec); lb/(ft)(sec)

$\nu$ blade-jet speed ratio (based on rotor-inlet tip speed), $U_t/V_j$

Subscripts:

cr condition corresponding to Mach 1

eq equivalent

w outer wall

t tip

1 station at turbine inlet (fig. 4)

2 station at stator exit

3 station at rotor exit

Superscripts:

' absolute total state

* U.S. standard sea-level conditions (temperature = 288.15 K (518.67$^{o}$ R), pressure = 10.13 N/cm$^{2}$ (14.70 psia))

# APPENDIX B

## LOSS ANALYSIS

An analysis was made to determine the magnitude of the various losses for each configuration investigated. The method described in reference 1 involved the determination of the velocity diagrams for each configuration at design speed and pressure ratio (design blade-jet speed ratio). The diagrams were determined from measured work, mass flow, inlet pressure and temperature conditions, speed, stator throat area, and the results of rotor-exit surveys of total pressure and flow angle. Design loss distribution between the stator and rotor was used to proportion the measured overall turbine loss for the 100-percent configuration. Stator losses for the other configurations were then assumed to vary in proportion to the average of the inlet and outlet kinetic energy levels as determined from the velocity diagrams. Included in the stator losses are the trailing-edge blockage losses, which increase as the stator throat area was decreased, and the scroll loss. The rotor incidence loss is assumed, as in the case of axial-flow turbines, to be equivalent to the kinetic energy of the relative velocity component normal to the blade at the rotor inlet. The nondimensional constants used in determining stator and rotor viscous loss was determined by the procedure described in reference 3.

Figure 24 shows the results of the calculations for all of the stator-rotor configurations investigated for operation at design blade-jet speed ratio.

Figure 24(a) shows the results of these calculations for the cases with the design rotor. The various losses, expressed in terms of efficiency, are shown as functions of specific speed. The magnitude of the exit kinetic-energy loss is shown by the difference between total and static efficiency values obtained at design blade-jet speed ratio for each stator configuration. The figure shows that the scroll-stator losses increase with decreasing specific speed. The increase in losses results from the increase in stator gas velocity as well as from increased trailing-edge blockage as stator throat area was decreased. Rotor losses decrease with decreasing specific speed at the high end of the specific speed range. The decrease in loss results primarily from the decrease in velocity level through the rotor as specific speed was decreased. Rotor incidence loss was essentially constant over most of the range of specific speeds covered in the investigation. Figure 24(b) shows the variation of turbine losses with specific speed for the tests with the rotor exducer extension. Scroll-stator losses increase with decreasing specific speed. Again, the losses increased because of the increase in stator gas velocity as well as the increased stator trailing-edge blockage as specific speed or stator throat area was decreased. Rotor losses increased as specific speed was increased

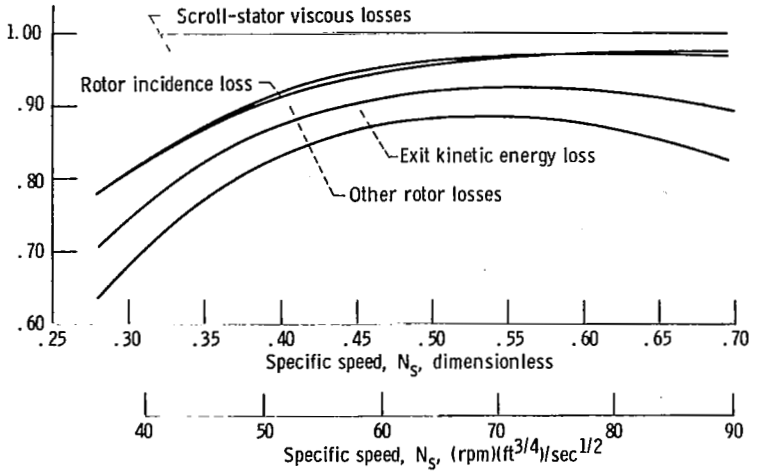


(a) Design rotor.

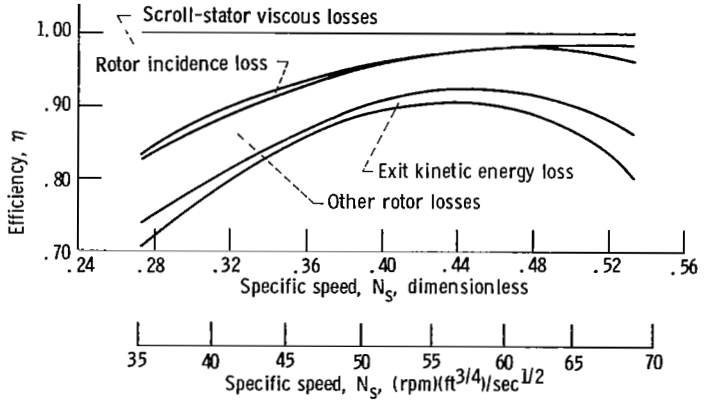


(b) Rotor extension.

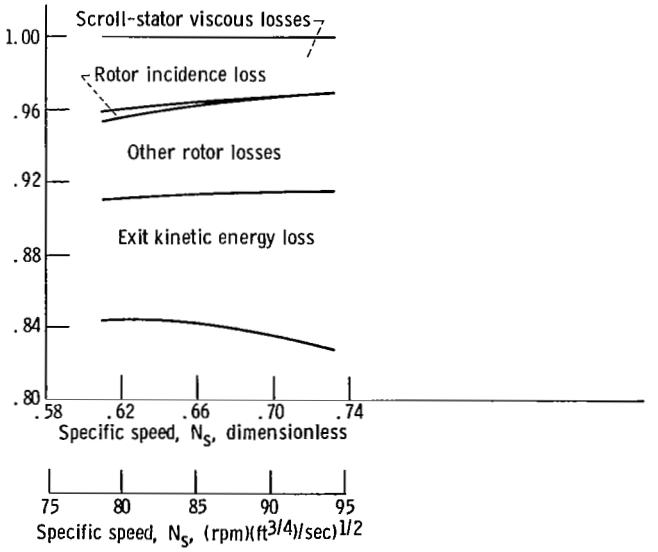


(c) Cutback rotor.

Figure 24. - Variation of turbine losses with specific speed at equivalent design speed and pressure ratio.

from about 0.42 to 0.53 (54 to 69). This would indicate an increase in relative velocity level through the rotor as specific speed was increased in this speed range. Rotor incidence losses were zero in the specific speed range of about 0.42 to 0.49 (54 to 63).

Figure 24(c) shows the variation of turbine losses with specific speed for the tests with the cutback rotor. For these tests the 100-, 125-, and 144-percent stators were used with the cutback rotor having a throat area 137 percent of design.

Comparison of the losses determined from the test results for the rotor configurations investigated illustrates the effect of stator-rotor throat area match. Scroll-stator loss was predominant with the rotor extension in the lower specific speed range. Rotor loss was the predominant loss over the entire specific speed range for operation with the cutback rotor configuration.

# APPENDIX C

## VELOCITY DIAGRAMS

Figure 25 shows the calculated velocity diagrams for all stator-rotor configurations investigated. These velocity diagrams were calculated at equivalent design speed and pressure ratio and using the results of the rotor exit surveys.

Figure 25(a) shows the velocity diagrams for the stator configurations investigated with the design rotor. The figure shows the expected flattening of stator exit velocity diagram as the stator throat area was decreased. It should be remembered that the same blade profile was used and that the blade setting angle was changed to obtain the various stator throat areas. The rotor velocity diagrams show a decrease in relative velocity through the rotor as stator throat area was decreased. The decrease in rotor-exit relative velocity with a constant wheel speed resulted in rotor-exit absolute flow angle becoming more positive with decreasing stator throat area. This was shown by the rotor discharge angle surveys discussed previously. The relative exit velocity level, for a given stator throat area, was higher for the rotor extension than for the design rotor or the cutback rotor. This was to be expected since the rotor extension gave a rotor throat area that was about 53 percent of design throat area.

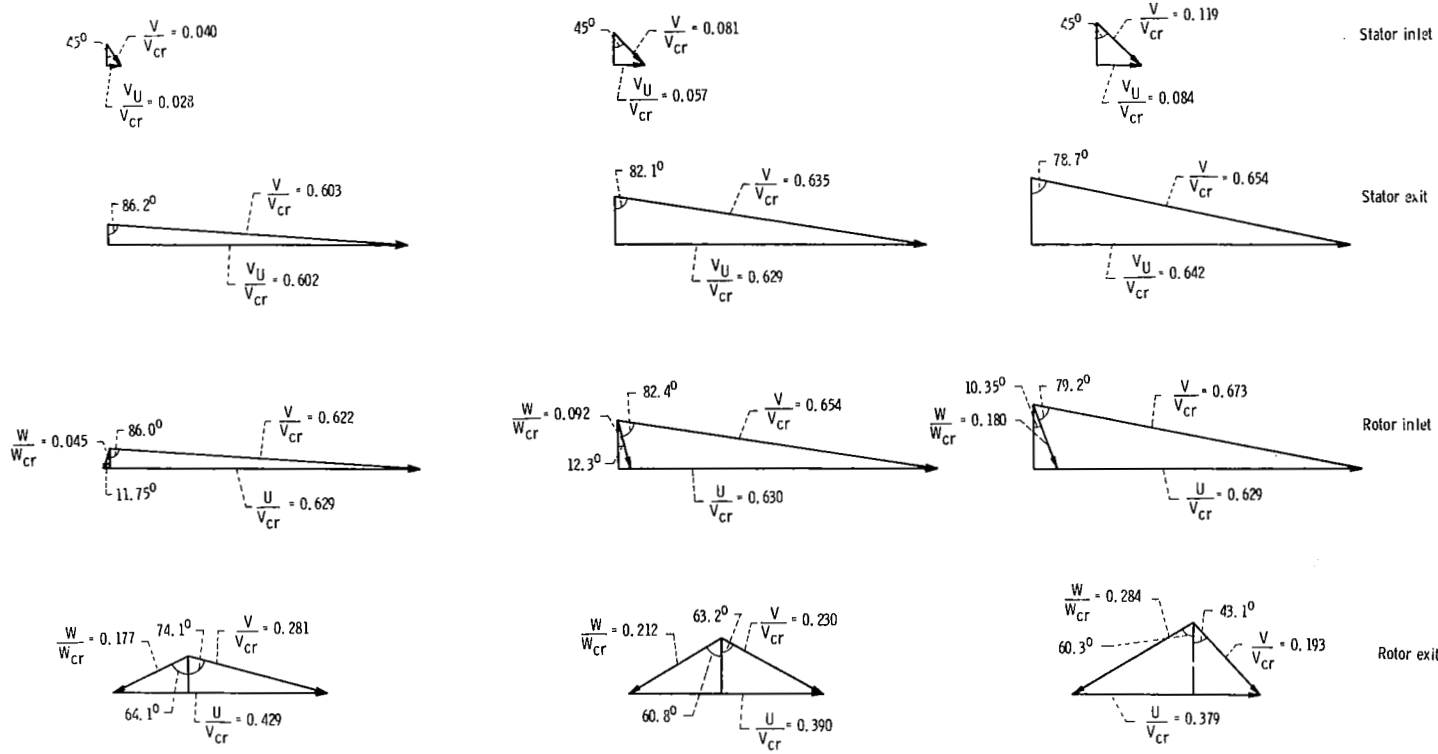


(a) Design rotor.

Figure 25. - Turbine velocity diagrams for stator configurations investigated at equivalent design speed and pressure ratio.

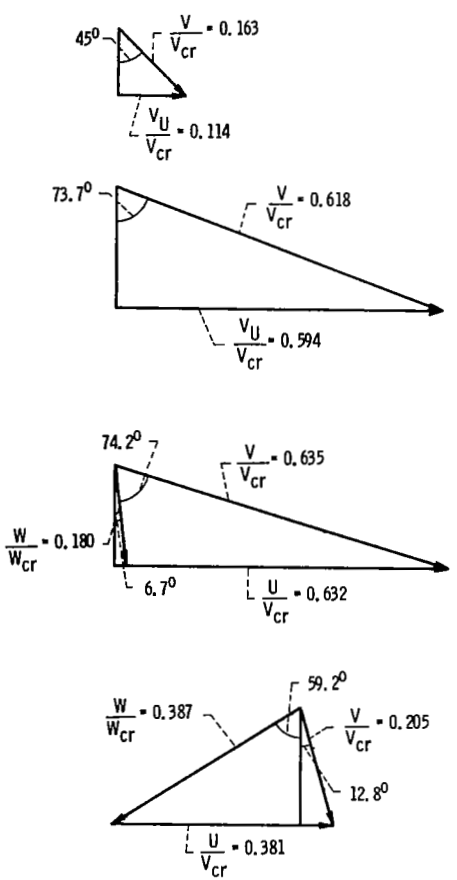


100-Percent stator throat area

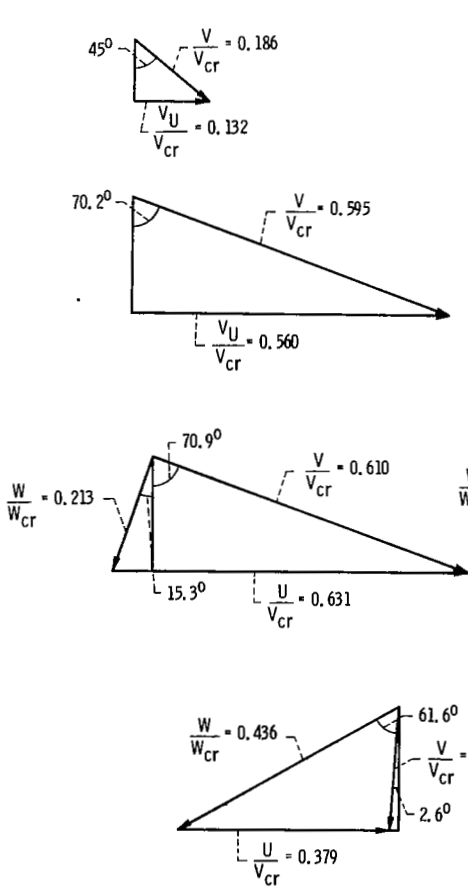


125-Percent stator throat area

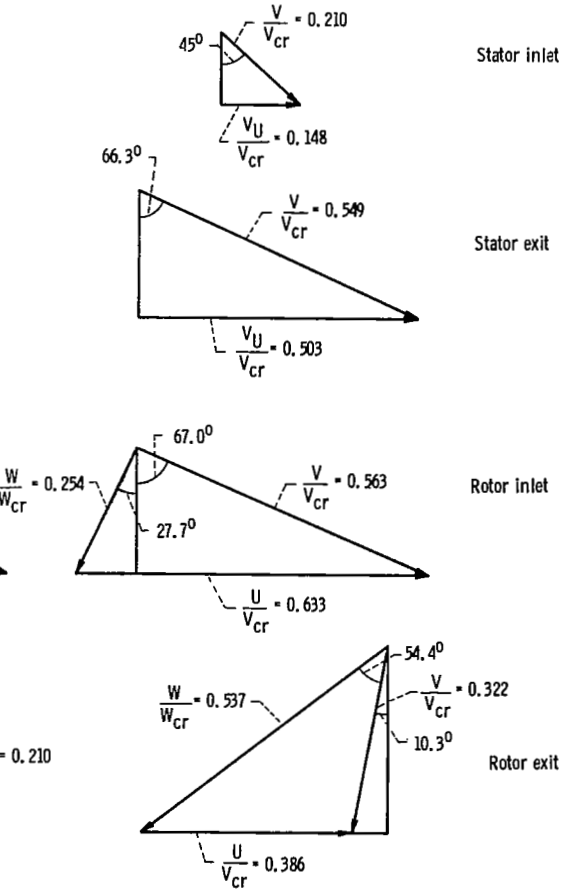


144-Percent stator throat area

(a) Concluded.

Figure 25. - Continued.

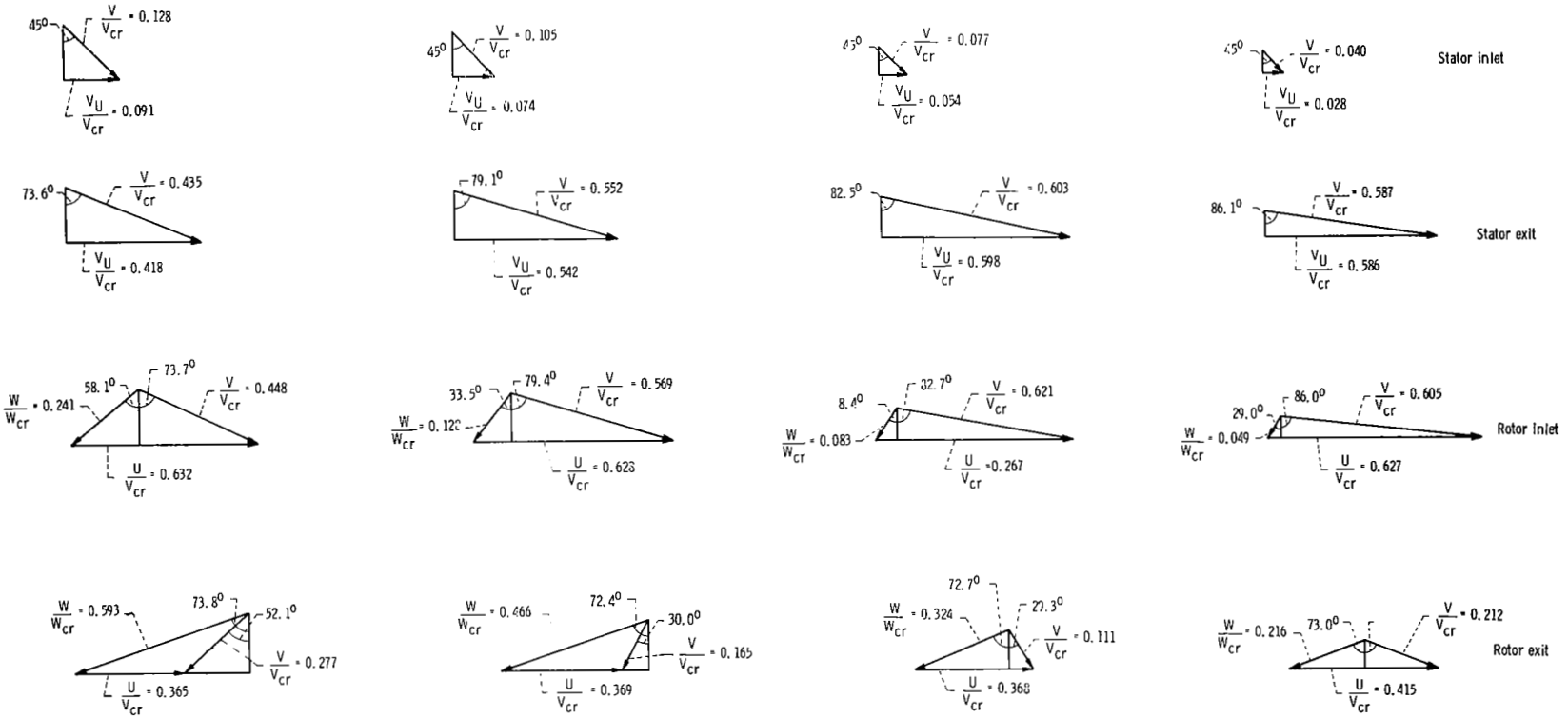


(b) Rotor extension.

Figure 25. - Continued.

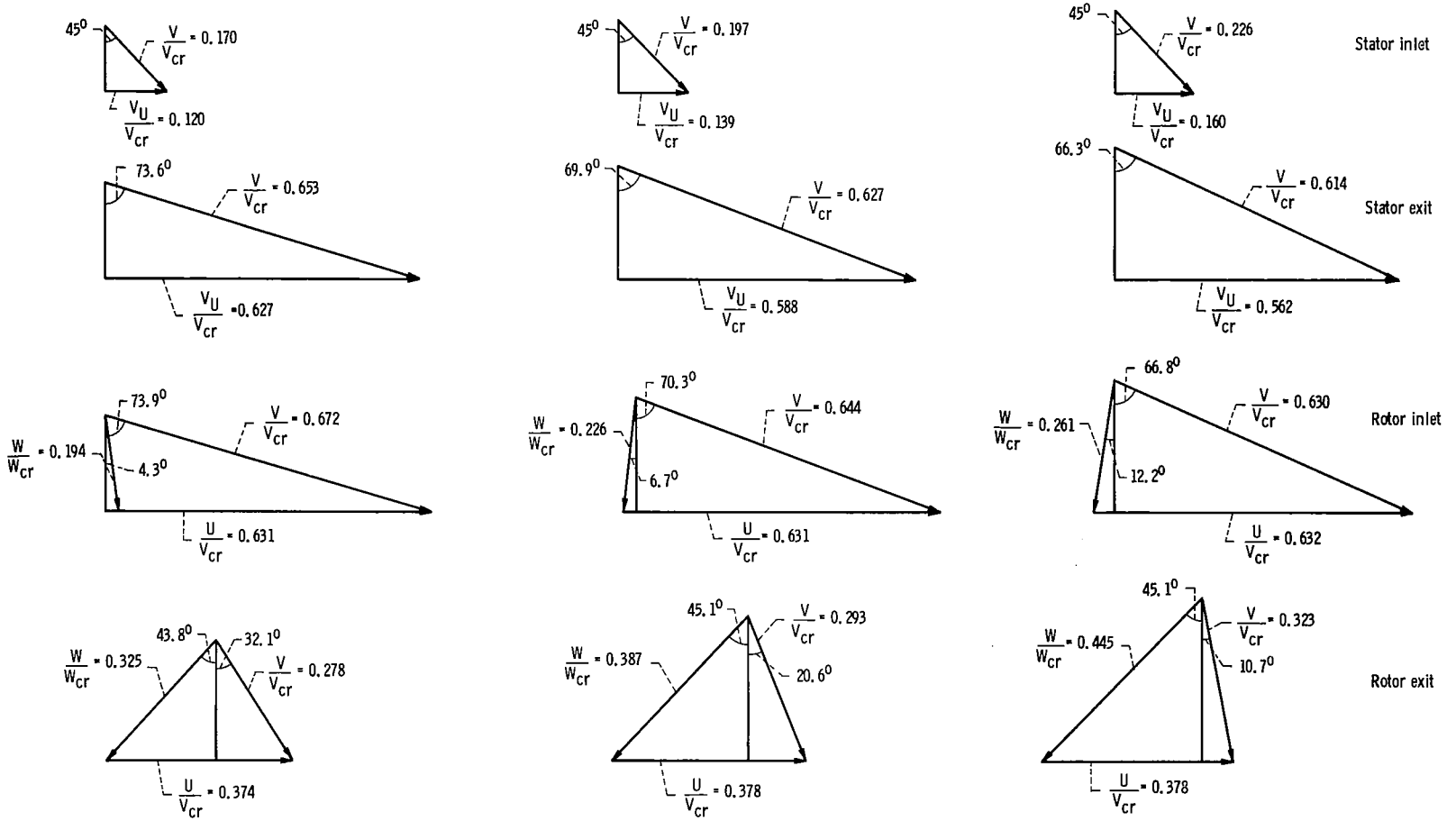


(c) Cutback rotor.

Figure 25. - Concluded.

# APPENDIX D

## BLADE SURFACE VELOCITIES

Figures 26 to 28 show the hub, mean, and tip rotor blade surface velocities for all stator and rotor configurations investigated. The rotor blade surface relative velocities were calculated by the method described in reference 4.

All rotor configurations showed negative pressure surface relative velocities for the 20-, 42-, and 66-percent stator configurations. Negative pressure surface velocities were obtained over the entire blade hub surface for the 20-percent stator configuration with the design rotor and the rotor extension case. Although the 42- and 66-percent stator configurations showed negative pressure surface velocities, which indicate a flow eddy, there were no large losses as evidenced by the high turbine performance with

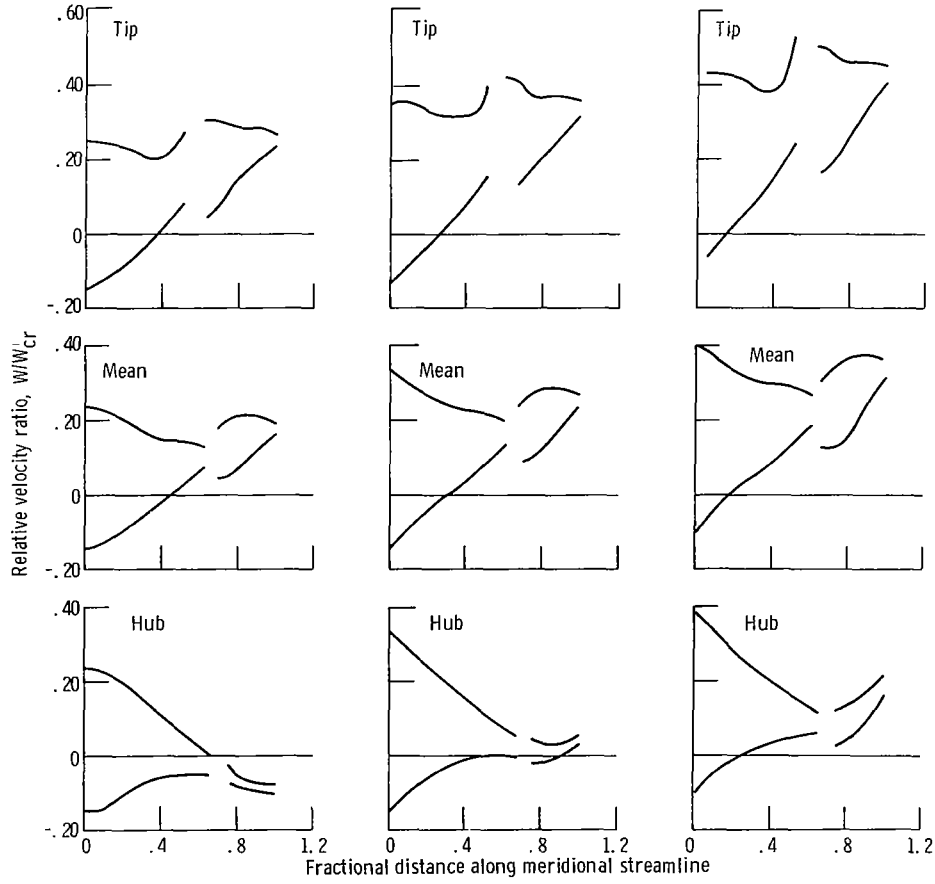


(a) 20-Percent stator throat area.

(b) 42-Percent stator throat area.

(c) 66-Percent stator throat area.

Figure 26. - Blade surface velocities at equivalent design speed and pressure ratio, design rotor.

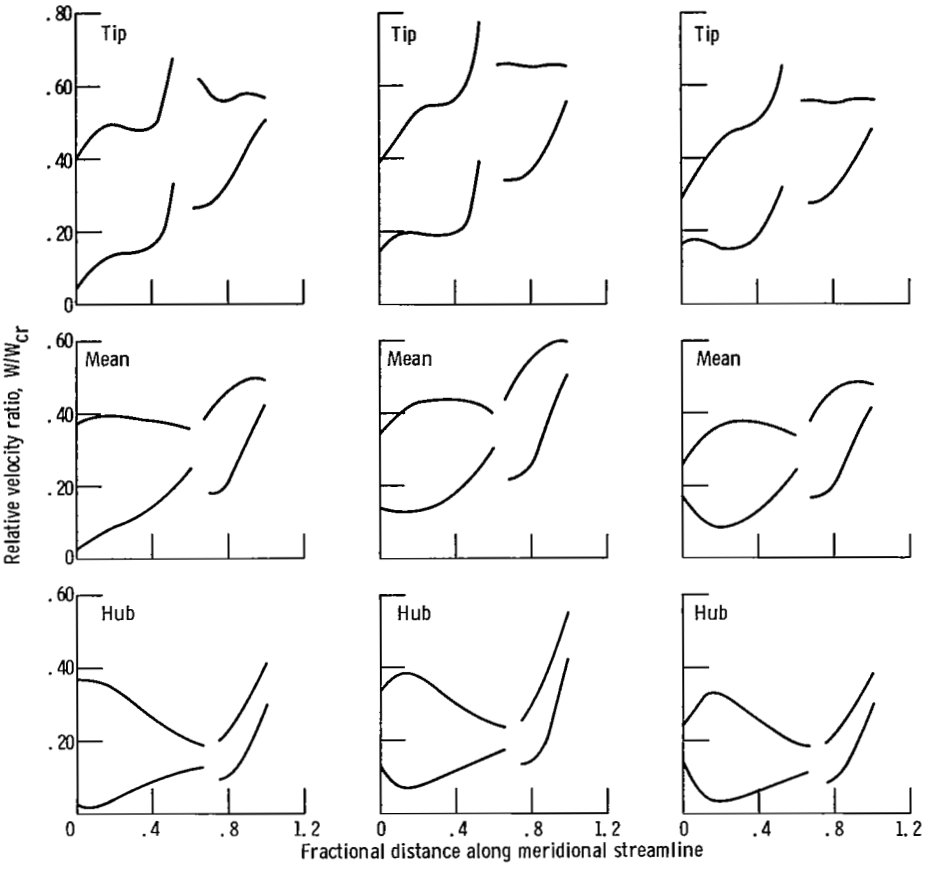


(d) 100-Percent stator throat area.

(e) 125-Percent stator throat area.

(f) 144-Percent stator throat area.

Figure 26. - Concluded.

these stator configurations. Negative pressure surface velocities over the entire blade hub surface for the 20-percent stator configuration could have resulted in flow separation for this stator configuration. This is evidenced by the rapid drop in turbine performance as well as the measurement of rotor exit flow angles greater than $90^{o}$ from axial. The flow angles would indicate flow separation with backflow in the hub region for the 20-percent stator configuration. Although the best rotor throat area was not obtained for the 20-percent stator configuration, we feel that the large drop in turbine performance cannot be entirely attributed to the poor stator-rotor throat area ratio.

The figures show no significant change in blade loading in comparing the results of the stator configurations for a given rotor configuration. Generally, the level of the relative velocities increased with increasing stator throat area.

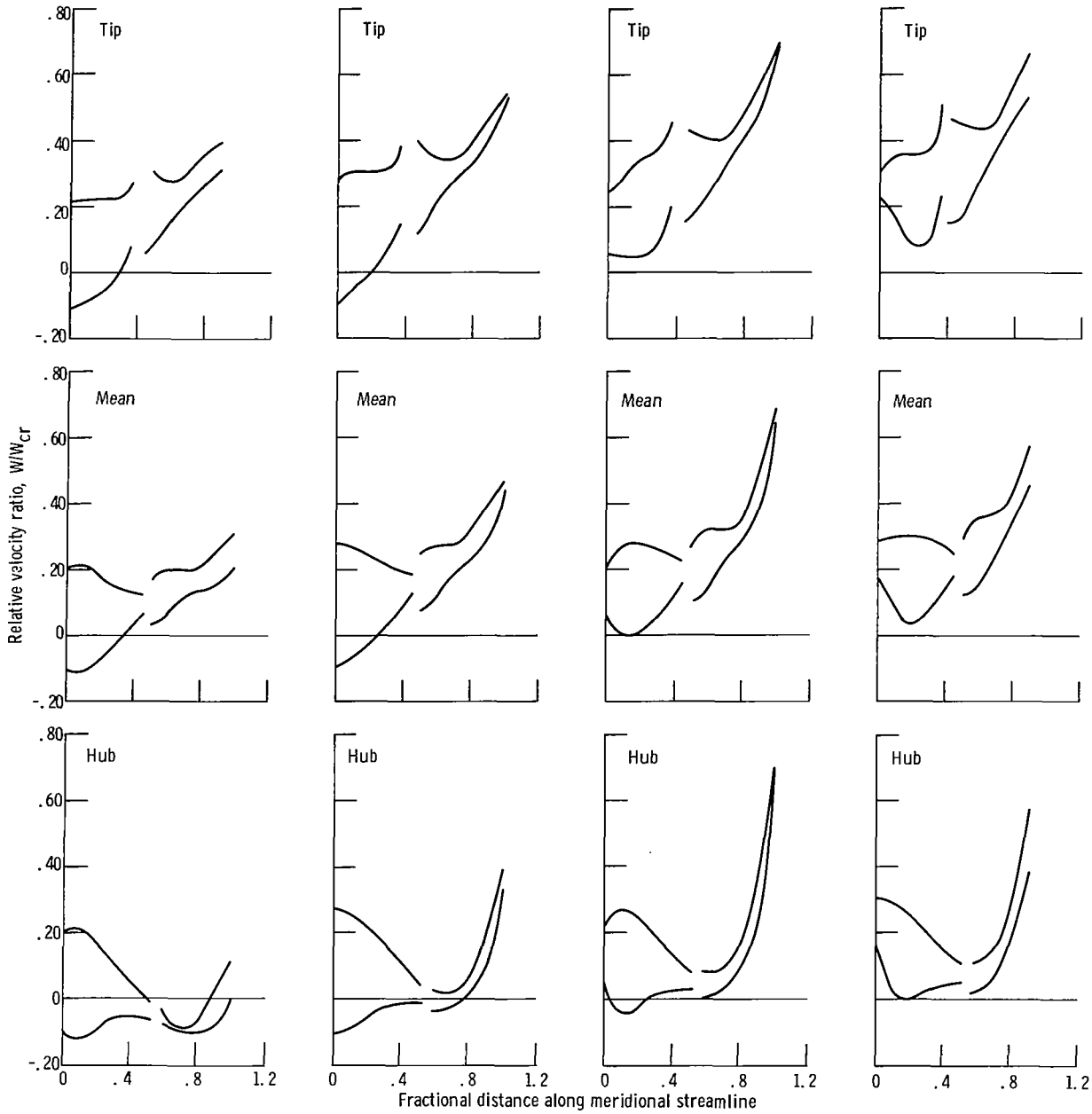


(a) 20-Percent stator throat area.

(b) 42-Percent stator throat area.

(c) 66-Percent stator throat area.

(d) 100-Percent stator throat area.

Figure 27. - Blade surface velocities at equivalent design speed and pressure ratio; rotor extension.

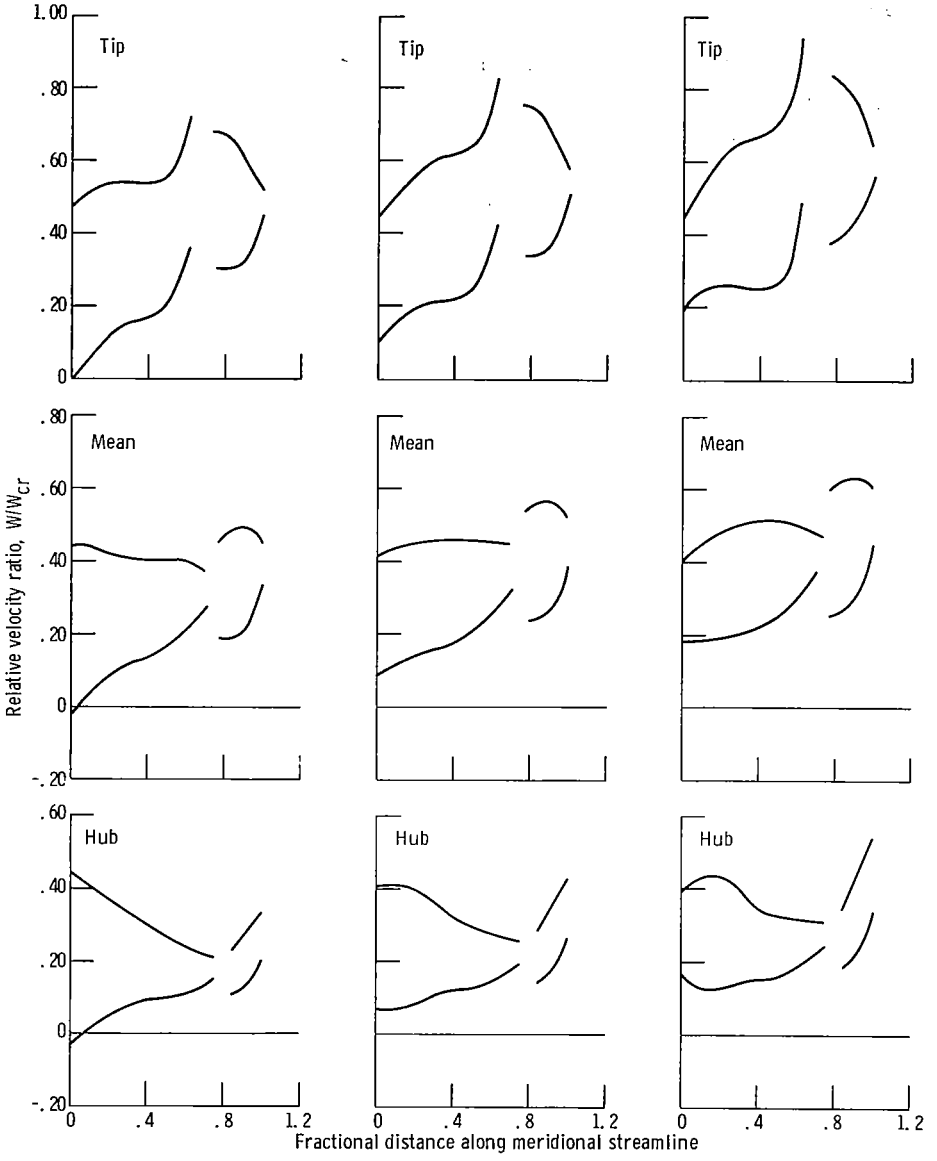


(a) 100-Percent stator throat area.

(b) 125-Percent stator throat area.

(c) 144-Percent stator throat area.

Figure 28. - Blade surface velocities at equivalent design speed and pressure rate; cutback rotor.

## REFERENCES


1. Kofskey, Milton G.; and Wasserbauer, Charles A.: Experimental Performance Evaluation of a Radial-Inflow Turbine Over a Range of Specific Speeds. NASA TN D-3742, 1966.

2. Nusbaum, William J.; and Kofskey, Milton G.: Cold Performance Evaluation of 4.97-Inch Radial-Inflow Turbine Designed for Single-Shaft Brayton Cycle Space-Power System. NASA TN D-5090, 1969.

3. Futral, Samuel M., Jr.; and Wasserbauer, Charles A.: Off-Design Performance Prediction With Experimental Verification for a Radial-Inflow Turbine. NASA TN D-2621, 1965.

4. Katsanis, Theodore: Use of Arbitrary Quasi-Orthogonals for Calculating Flow Distribution in the Meridional Plane of a Turbomachine. NASA TN D-2546, 1964.




NASA-Langley, 1972 —— 3 E-6349